Sādhanā, Vol. 10, Parts 3 & 4, August 1987, pp. 459–495. © Printed in India

Some aerodynamic problems of satellite launch vehicles

T S PRAHLAD

Flight Dynamics Group, Vikram Sarabhai Space Centre (VSSC), Trivandrum 695 022, India

Present address: Aeronautical Development Agency (ADA), NAL Campus, Belur, Bangalore 560 037, India

Abstract. A Satellite Launch Vehicle, during its atmospheric flight, presents a variety of aerodynamic problems for which solutions are to be obtained through analytical and experimental techniques. Generally, the problems are complex and three-dimensional in nature and quite often involve multibody interactions, interactions between the free stream and propulsive jet etc.

In this paper, attention is confined to the current aerodynamic problems of interest to VSSC in relation to the Augmented and Polar Satellite Launch Vehicles under development. Aerodynamically, these are multibody configurations with strap-on boosters and have bulbous payload shrouds. Five important problem areas, namely, vehicle lift-off, strap-on aerodynamics, strap-on separation, stage-separation aerodynamics and boat-tail aerodynamics are selected for presenting some of the recent work done in VSSC using both computational and experimental methods. The main emphasis is on results and applications rather than on details of the methods used.

Keywords. Launch vehicles; space technology; strap-on vehicles; stage separation; jet interactions; boat-tailed bodies.

1. Introduction

A satellite launch vehicle (SLV), from the time of its lift-off to the time it leaves sensible atmosphere, poses a variety of aerodynamic problems from subsonic to hypersonic speeds. The subject is quite vast and there is a considerable amount of literature starting from the earlier Scout type of launch vehicle to the current Space Shuttle. In this presentation, attention is confined to the Indian experience and also to some of the more recent work that is being carried out in selected areas in VSSC on configurations of interest to the Indian space programme.

India successfully entered the field of indigenous satellite launch vehicle development on 18 July 1980, when a 23 m long four-stage solid propellant rocket SLV-3 launched the 40 kg Rohini satellite into a low earth elliptical orbit. SLV-3,

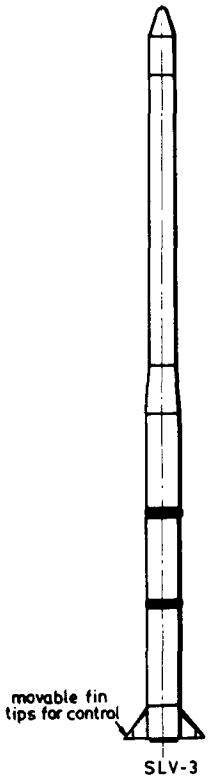

Figure 1. Aerodynamic configuration of SLV-3.

shown in figure 1, was a simple aerodynamic configuration with a blunt cone and a flared interstage between the first and the upper stages. It had four fins to provide aerodynamic stability as well as to provide aerodynamic control with movable fin tips during the first-stage flight.

After three successful flights of SLV-3, attention has now turned to the development of two new satellite launch vehicles – the Augmented Satellite Launch Vehicle (ASLV) and the Polar Satellite Launch Vehicle (PSLV). These are shown schematically in figure 2. In ASLV, two strap on boosters are added to the basic SLV-3, but without the fins, to act as the first stage of a five-stage vehicle to increase the payload capability from 40 to 150 kg in low earth orbit. The payload shroud is increased in diameter from 800 mm to 1000 mm leading to a bulbous configuration. The PSLV is a vehicle that is being developed for launching a 1000 kg satellite in a 900 km sun-synchronous orbit for purposes of Indian resources survey. It is of 2·8 m diameter with 6 strap-on boosters of 1 m diameter which augment the thrust at take-off. Aerodynamically, complexity arises again because of the strap-on boosters and the bulbous (bulb-shaped) payload shroud (also referred to as heat shield) necessary for accommodating the payload.

While many routine aerodynamic design, analysis and testing tasks are being tackled for both ASLV and PSLV, five important problem areas, as indicated in figure 2, are selected here for further discussion. These are of interest not only for the present launch vehicle programmes of VSSC, but also for future vehicles like the Geosynchronous Satellite Launch Vehicle (GSLV) which will continue to use

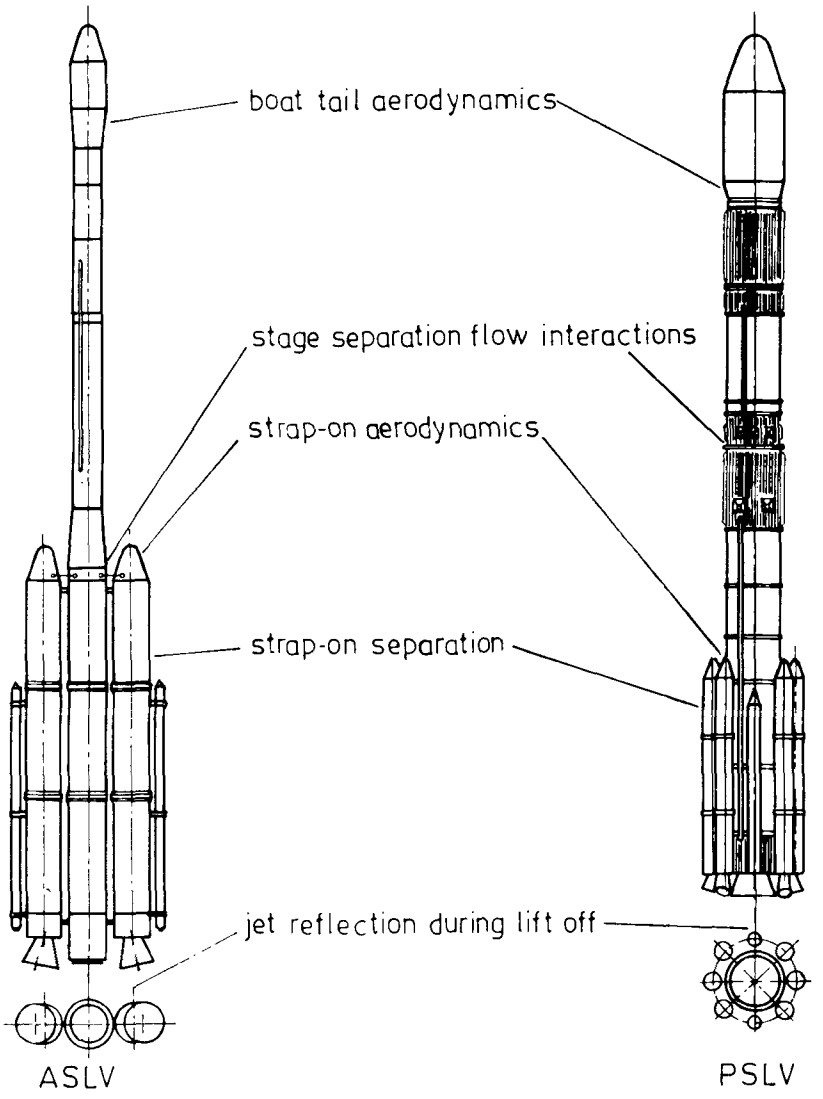

Figure 2. Aerodynamic configurations of ASLV (Augmented Satellite Launch Vehicle) and PSLV (Polar Satellite Launch Vehicle) and important problem areas (not to scale).

concepts like strap-on staging, bulbous payload shrouds etc. Many of the studies indicated here are still in progress and further work needs to be done, especially as regards detailed experimental validation of the computational codes under development. In some cases, efforts have been directed mainly towards providing an engineering answer to a complex design problem. Deeper investigation of the scientific aspects needs to be taken up. Also, emphasis here is on the presentation of results for problems of interest, rather than on a detailed discussion of methods.

2. Vehicle lift-off

Jet interaction with the launch pad, as well as the vehicle itself, constitutes an important and complex fluid dynamic problem during the lift-off of a launch vehicle. The design aspects to be considered are the following:

(a) diversion of the jet or jets away from the launch pad through a suitable jet deflector where necessary;
(b) pressure and thermal loads on the jet deflector required for the design of the deflector;
(c) acoustic load distribution along the length of the vehicle caused by reflection from the launch pad and ensuring that the vehicle subsystems can withstand these loads.

These aspects have been considered here through a combination of semi-empirical methods and subscale experiments.

Figure 3 illustrates the lift-off fluid dynamic problem for ASLV where the two strap-on jets impinge on a flat surface. The central fountain formation has been studied in a subscale cold flow experiment (J K Prasad 1984, private communication). The Mach number distribution, as a function of distance from the impingement surface, indicates that the central fountain does not reach upto the vehicle base and so poses no problem during lift-off in the present case.

However, for PSLV, which employs a much larger solid booster and where both the core and the strap-on boosters are ignited at lift-off, it was decided to provide a

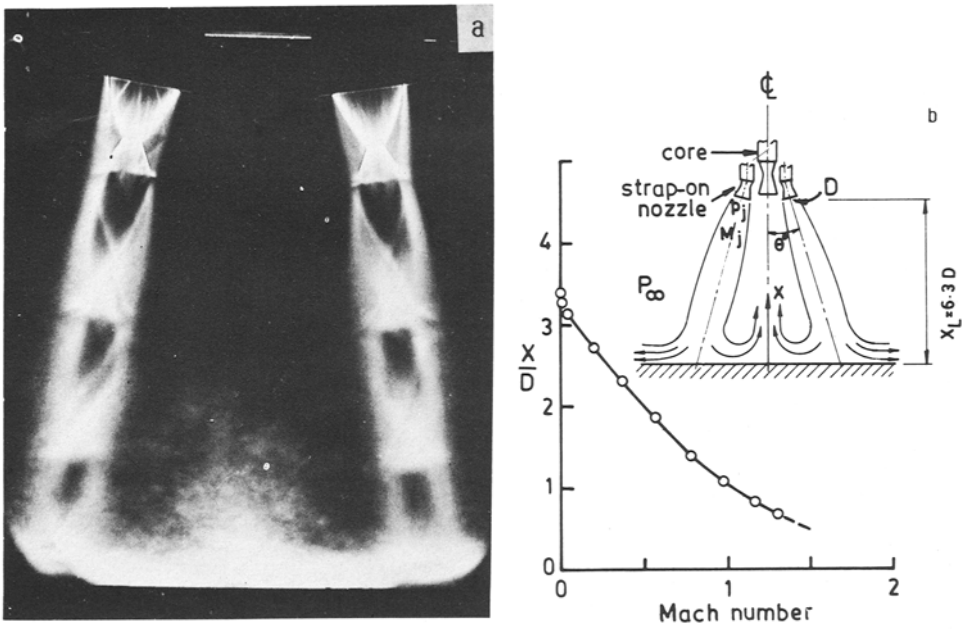

Figure 3. Lift-off fluid dynamic problem of ASLV: Two strap-on jets impinging on a flat surface **(a)** Schlieren view **(b)** Centre line velocity distribution in fountain jet: $M_j = 2{\cdot}98$; $X_L/D = 6{\cdot}3$; $p_j/p_\infty = 0{\cdot}5$.

suitable jet deflector. Taking into account various launch site and launch tower constraints, two deflectors – a double wedge type and an inclined plate type – were taken up for detailed investigation. Figure 4 is a schematic of the flow field due to the impingement of the core and the strap-on jets on a double wedge deflector. The schilieren pictures, shown in figures 5a and b and taken during laboratory cold flow simulation tests on double wedge and inclined surface deflectors, represent the complexity of the flow field with interactions between shocks, core and strap-on jets and boundary layer (Prasad & Kutty 1985). Surface pressure distributions and wall jet velocity distributions were also measured in these tests in order to design the deflector foundation and to ensure that the exhaust is contained within the trench. Typical pressure distributions along the centre line and across the span of a double wedge deflector are shown in figure 6 from which one could obtain an estimate of deflector foundation loads. Velocity distributions measured in the diverted wall jet (figure 7) indicated that the wall jet height for the cold flow was less than $1D$, thus providing adequate margin even with temperature effects.

In order to design a suitable thermal protection system over the deflector for withstanding the heavy thermal loads during lift-off, recourse was again taken to subscale static tests using both double wedge and inclined plate types of deflectors (Anon 1985). The test set up is shown in figure 8. The jet deflector model had a 50 mm thick high temperature refractory coating on top of a steel plate with suitable anchorages. A typical erosion pattern can be seen in figure 9. Several tests were conducted on both types of deflectors with varying geometrical properties. The overall conclusion from these tests is that the erosion depth and the extent are roughly the same in both types of deflectors, though there are marginal differences. The erosion is of acceptable extent and repair would be possible from one launch to the next.

As far as acoustic loading is concerned, the overall sound pressure distribution along the length of the vehicle with jet deflector effects could only be estimated by

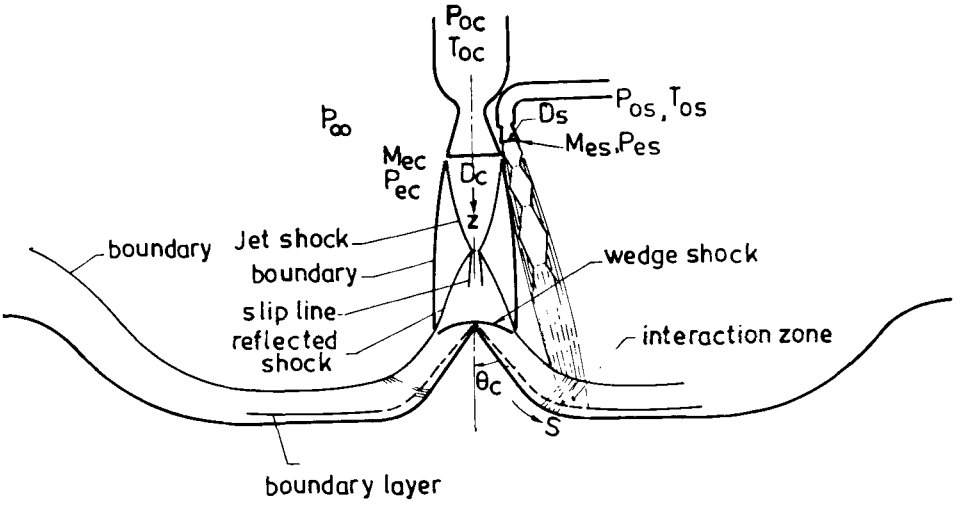

Figure 4. Schematic of the flow field due to core and strap-on jet impingement on double wedge deflector.

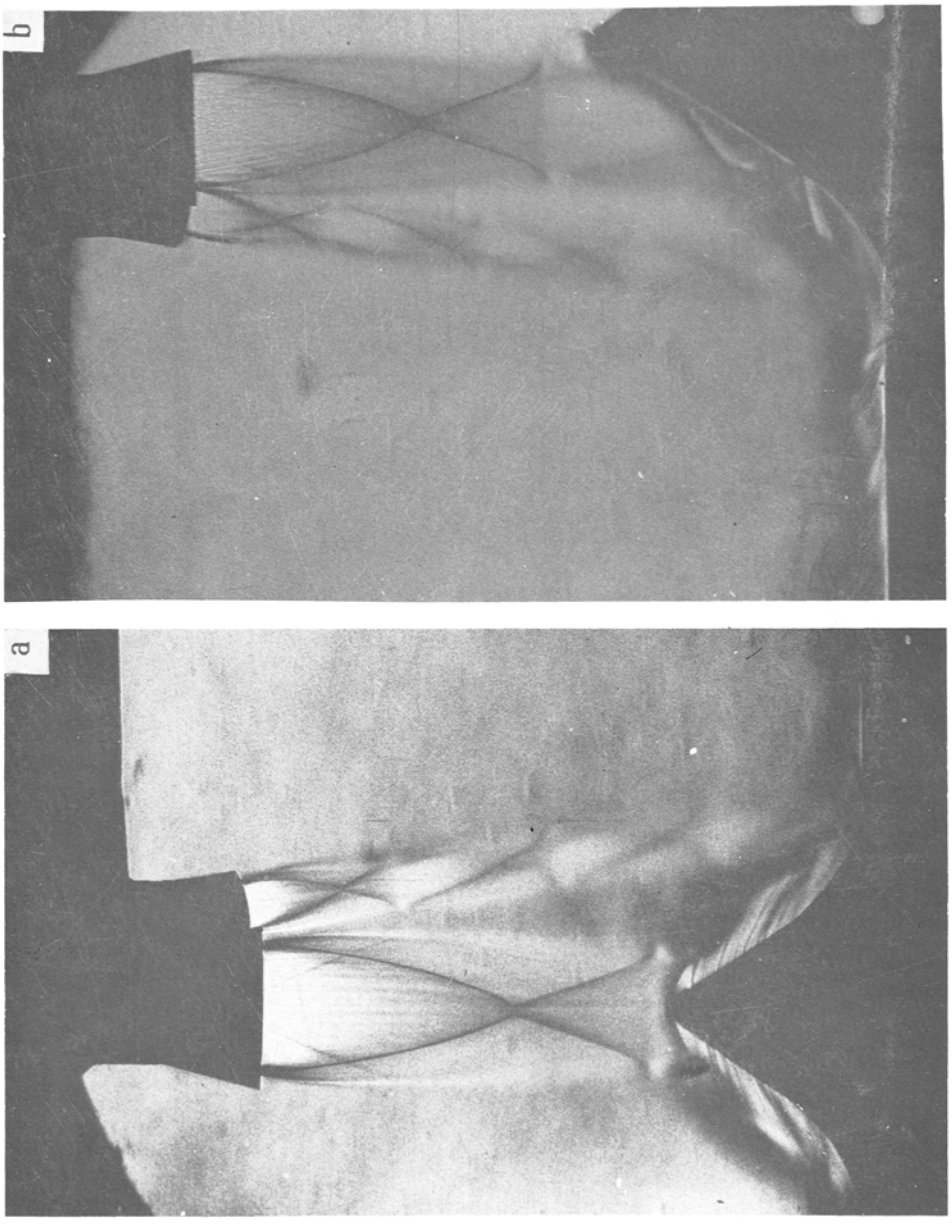

Figure 5. Schlieren pictures of core and strap-on jets impinging on (**a**) double wedge deflector and (**b**) single inclined surface deflector.

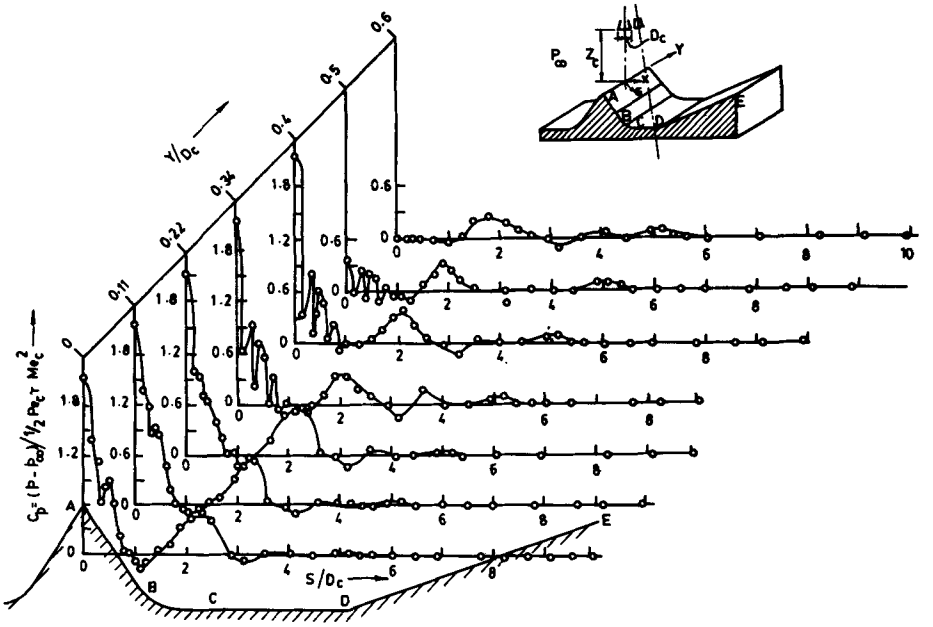

Figure 6. Typical pressure distribution along the centre line and across the span of a double wedge jet deflector, core jet Mach number Mec = 3·12, strap-on jet Mach number Mes = 3·0, core jet pressure ratio Pec/P_∞ = 0·88, strap-on jet pressure ratio Pes/P_∞ = 0·7, distance from exit plane of core nozzle Zc/Dc = 3·0, p = local static pressure, C_p = pressure coefficient, γ = specific heat ratio.

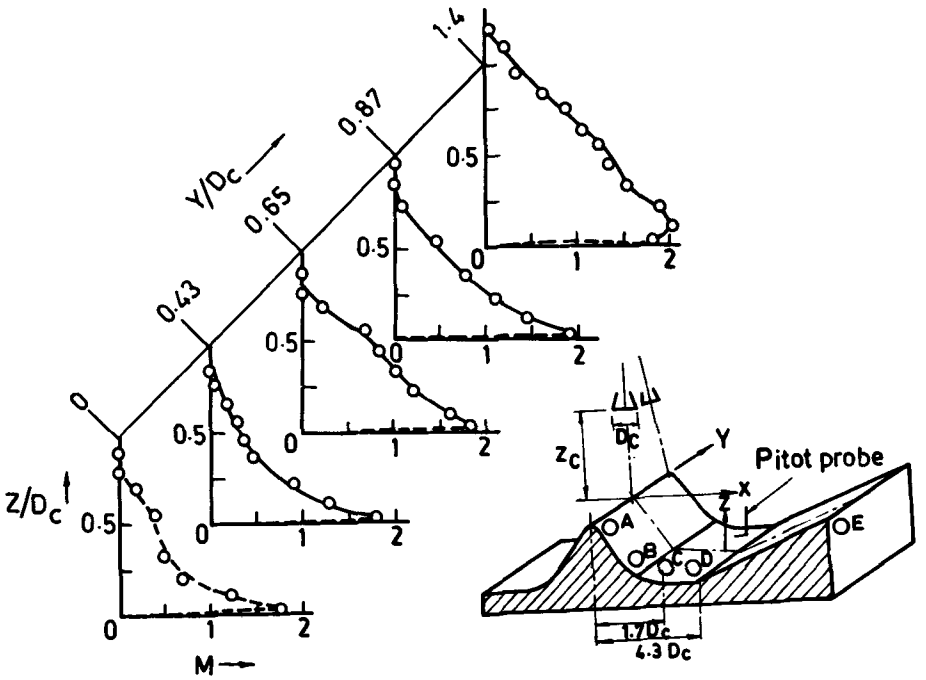

Figure 7. Spanwise variation of Mach number M in the wall jet at x/Dc = 3·6; Other conditions same as for figure 6.

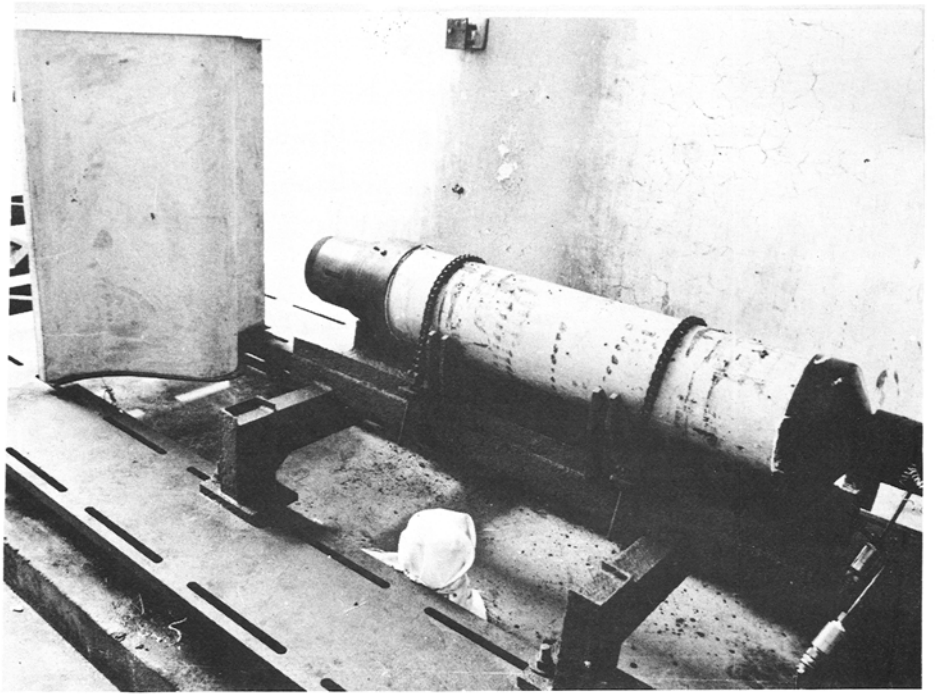

Figure 8. Static test set up with 200 mm diameter solid rocket motor and double wedge deflector with high temperature refractory lining.

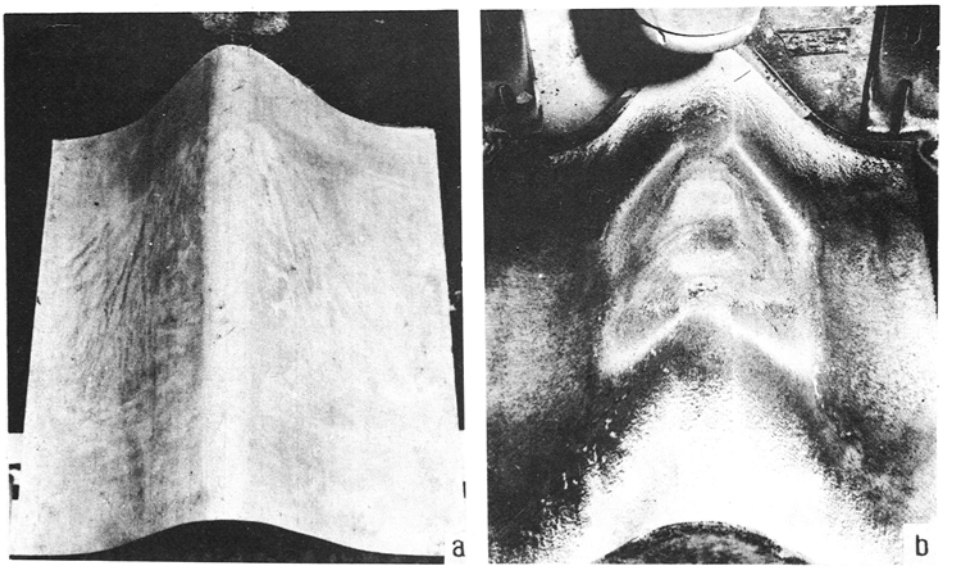

Figure 9. Double wedge deflector model **(a)** before and **(b)** after static test showing the erosion pattern.

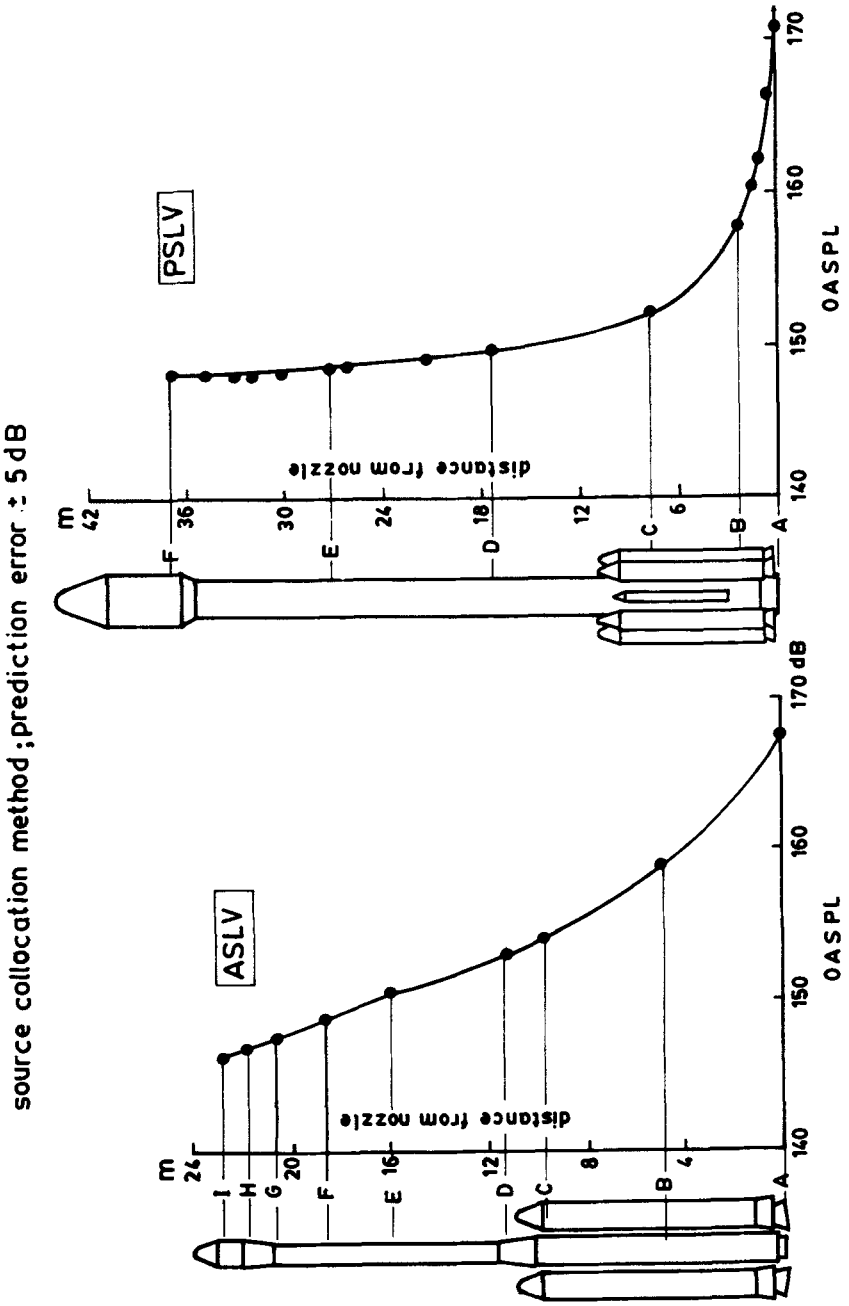

Figure 10. Overall sound pressure levels (OASPL) at various stations along the length of the vehicle during take-off.

approximate semi-empirical methods and such estimates are shown in figure 10 for ASLV and PSLV (M S Sastry 1986, private communication). There is need for refining the above estimates through subscale experimental work.

Thus, there is considerable complexity in the fluid dynamics problem that arises during the lift-off of a launch vehicle. Though one can tackle the specific design problems through a combination of suitably tailored subscale experiments and semi-empirical methods, there is clearly a need for obtaining a much better understanding of the fluid dynamic aspects involved and their effects on pressure loads, surface erosion, sound pressure levels etc. The newly emerging field of computational fluid dynamics can play a significant role in this along with carefully conduoted subscale experiments.

3. Strap-on aerodynamics

The aerodynamics of multibody configurations involving strap-on boosters has been receiving considerable attention in VSSC because of its relevance to current and future launch vehicle programmes. Methods are under development for subsonic, transonic and supersonic flow analysis involving two or more strap-on boosters. This section gives a brief account of these methods and the important results obtained.

3.1 *Subsonic flows*

The well-known panel method with surface singularity distribution and incompressible flow assumption is used for multibody configurations of interest. For ASLV, 800 panels have been used, along with symmetry considerations, and are distributed as shown in figure 11 (Devassia *et al* 1982, pp. 553–558). Computations were performed on the CDC CYBER 170/730 system of VSSC. Longitudinal pressure distributions along various generators for a given gap between the core and the strap-on as well as the circumferential pressure distribution are shown in figures 12 and 13 along with the experimentally measured static pressures. The conditions are not exactly identical as the test Mach number is arount 0·5 whereas computation assumes $M = 0$. Also, the model has connectors between the core and the strap-on which are not taken into account in the computation. Further, the computational method does not correct for viscosity. Taking all these factors into account, the agreement can be considered quite reasonable for purposes of preliminary design.

Integrating such pressure distributions calculated at the angle of incidence, aerodynamic load distributions have been obtained along the vehicle length for purposes of structural design. A typical load distribution is shown in figure 14. Similar computations have also been performed for PSLV with a larger number of strap-on boosters.

3.2 *Supersonic flows*

The flow field arising out of a supersonic free stream past a strap-on multibody configuration is shown in figure 15 which indicates the complexity of the fluid

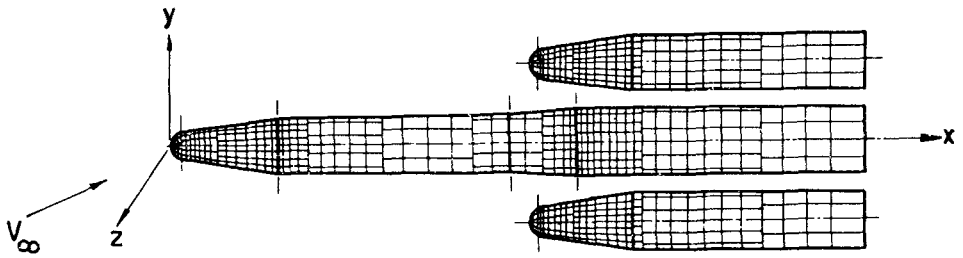

Figure 11. Distribution of panels for subsonic inviscid flow field calculation on a strap-on configuration. Note the various types of distributions at different longitudinal locations on the body. Circumferential distribution is adjusted to have elements of similar shape as for as possible.

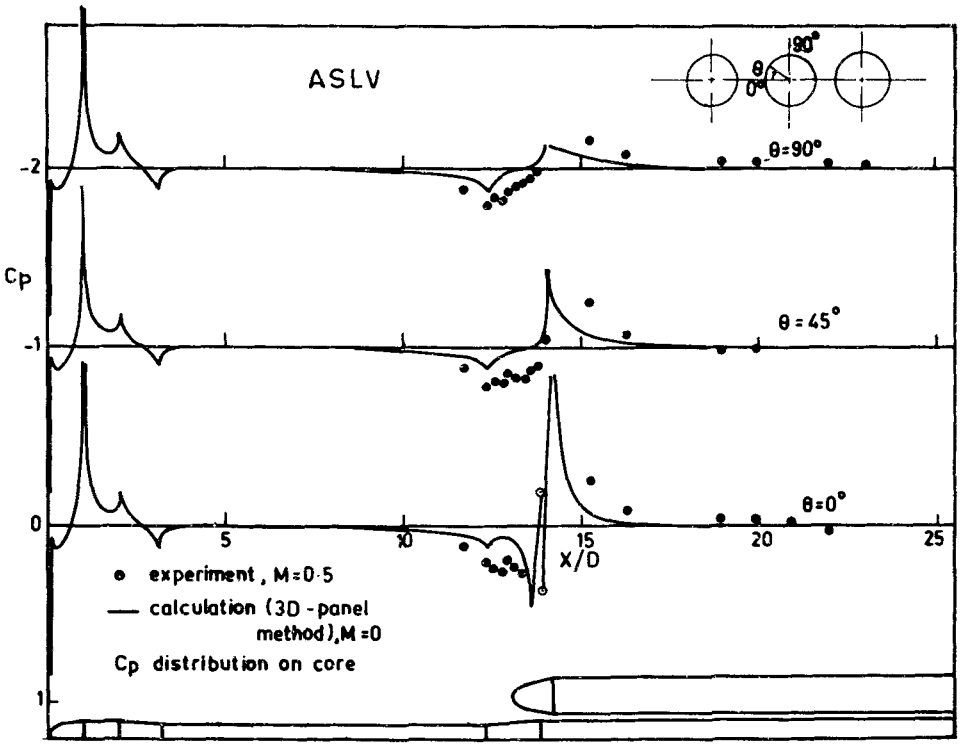

Figure 12. Pressure distribution along the length of the core vehicle; Comparison between computed and experimental results.

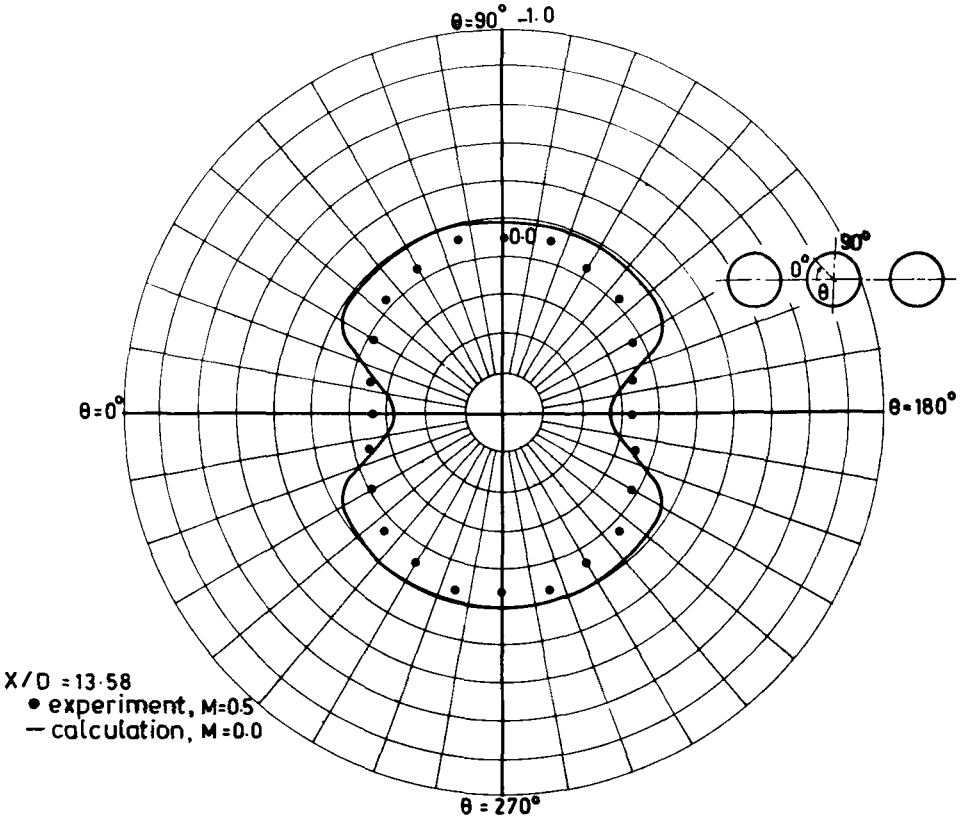

Figure 13. Typical circumferential pressure distribution on the core vehicle.

dynamic problem involved here with multiple shock interactions and reflections. The inviscid supersonic flow field governed by Euler equations is solved (Singh *et al* 1987) by a shock capturing scheme using MacCormack's (1969) second-order explicit predictor-corrector method. An 'overlap grid scheme' is used wherein the strap-ons and the core are wrapped in separate meshes such that there is an overlap region between the two grids (figure 16) where the core and the strap-on solutions can be interpolated. As there is no upstream influence in supersonic flows, the flow ahead of the strap-on upto plane AB (figure 15) is simulated about the core vehicle using a single grid scheme, and downstream of the plane AB the computation is carried out with the overlap grid. To capture strap-on shock and its reflection accurately, clustering of the grids was found necessary in the strap-on region both in the radial and in the circumferential directions.

Figure 17 shows a typical pressure contour in the strap-on region obtained from the above computation and figure 18 represents a computer-simulated schilieren. Figure 19 gives the longitudinal pressure distribution and figure 20 the aerodynamic loading distribution on the strap-on, one of the primary parameters of design

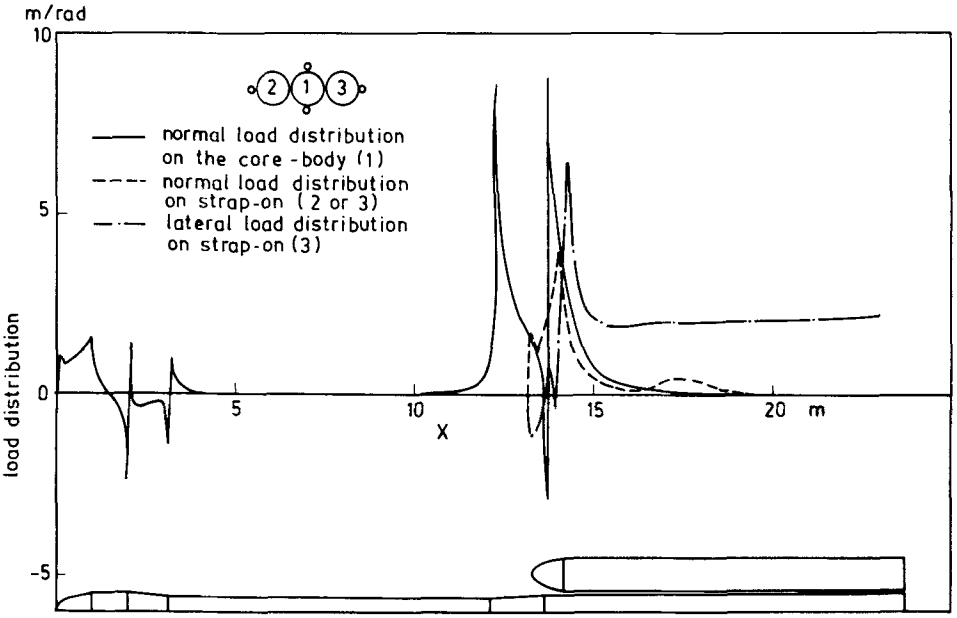

Figure 14. Typical aerodynamic load distributions on a strap-on configuration obtained by integration of surface pressure variation from the panel method.

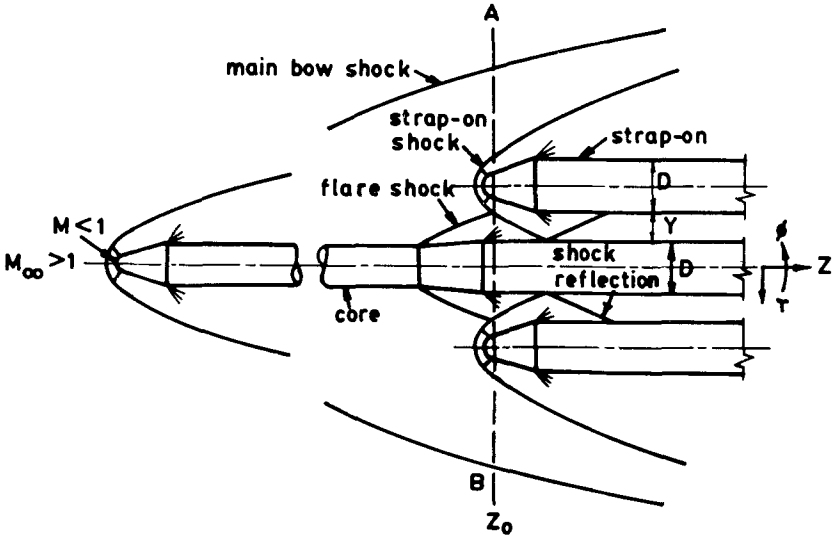

Figure 15. Schematic of supersonic flow field over launch vehicle with strap-on boosters.

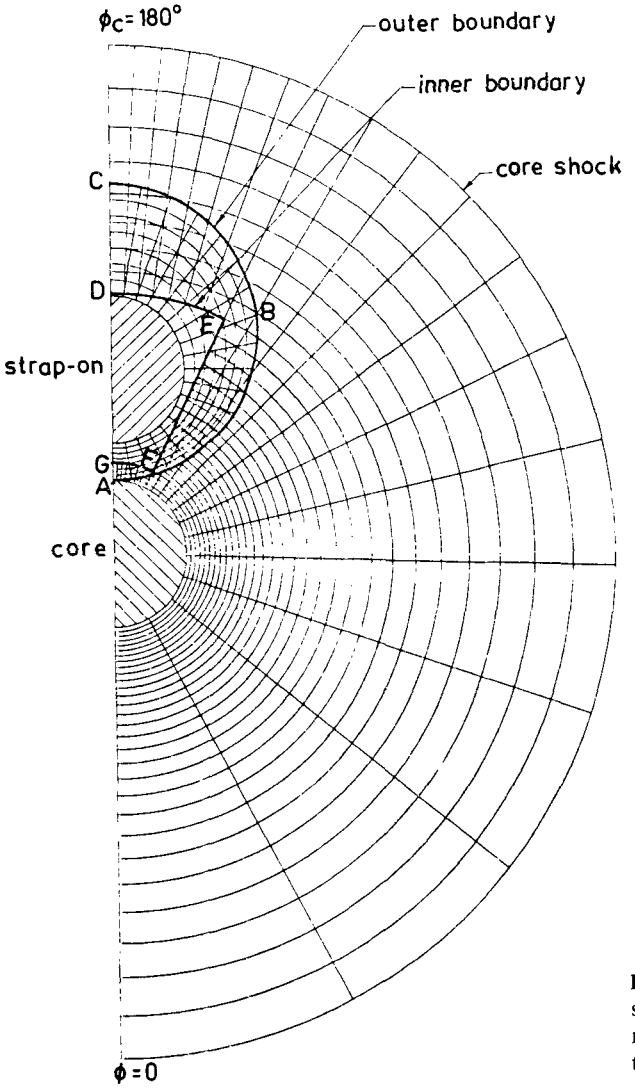

Figure 16. Grids for core and strap-on bodies with an overlap region ABCDEFG for interpolating the core and strap-on solutions.

interest. The different regions of the load distribution can be correlated to the impingement and reflection of the shocks and expansions arising in this region in supersonic flow. Another important parameter of design interest is the variation in side force acting on the strap-on as a function of distance from the core and is indicated in figure 21 as obtained through integration of the pressure distribution. A comparison made with limited wind tunnel results is encouraging though more detailed generation of experimental data and comparisons are called for. The trend indicates that viscous effects, ignored in the present calculation, are not likely to be very dominant (except perhaps for a narrow circumferential band around the generator facing the core vehicle) as far as overall force levels are concerned.

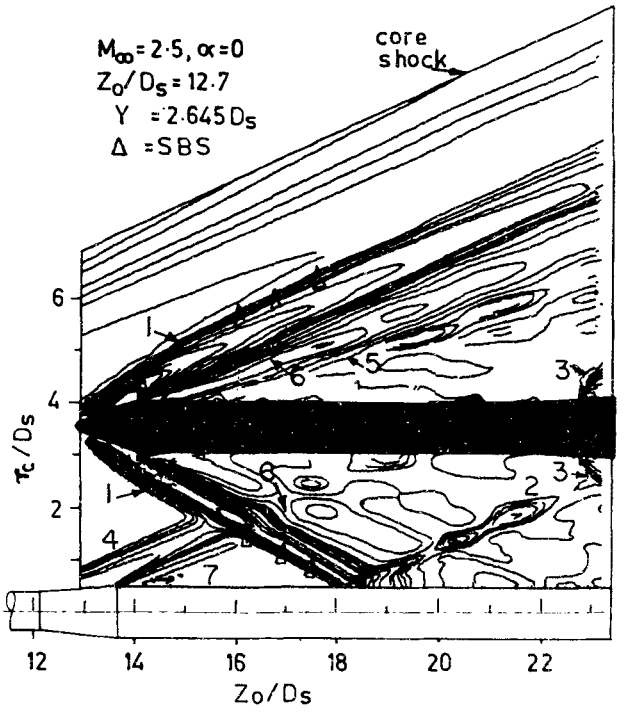

Figure 17. Pressure contours in the region of strap-on shock interference with the core; 1: Incident shock, 2: Reflected shock, 3: Strap-on flare shock, 4: Core flare shock, 5: Recompression shock, 6: Strap-on expansion fans, 7: Core expansion fans. SBS: Single body simulation method.

Similar work is in progress for the larger number of strap-ons in PSLV and the corresponding overlap grid scheme is indicated in figure 22.

While the above calculations are purely inviscid, viscous effects assume importance where the shock from the strap-on interacts with the core boundary

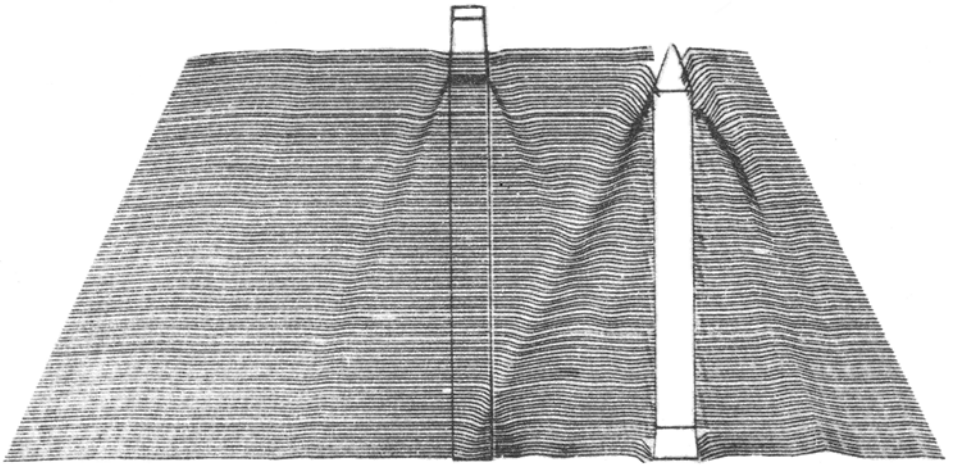

Figure 18. Typical computer simulated Schilieren for the interference region between core and strap-on: $M_\infty = 2{\cdot}5$, $\alpha = 0$, Gap = 4·145 D.

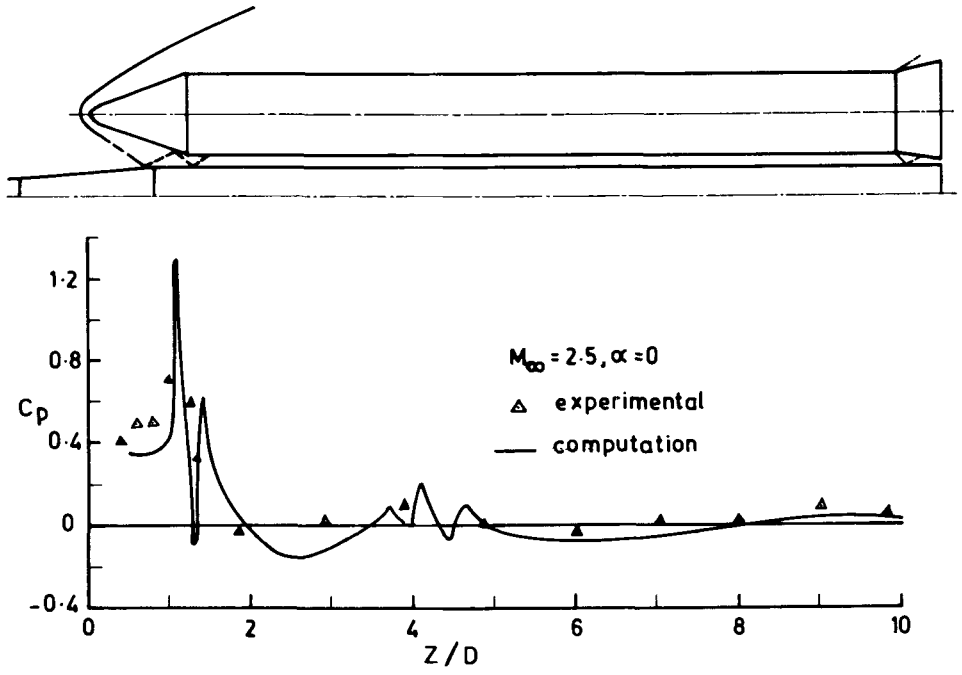

Figure 19. Longitudinal pressure distribution on the strap-on in comparison with experimental values M_∞ = free stream Mach number, α = angle of incidence, Cp = pressure coefficient, z = axial distance, D = strap-on body diameter.

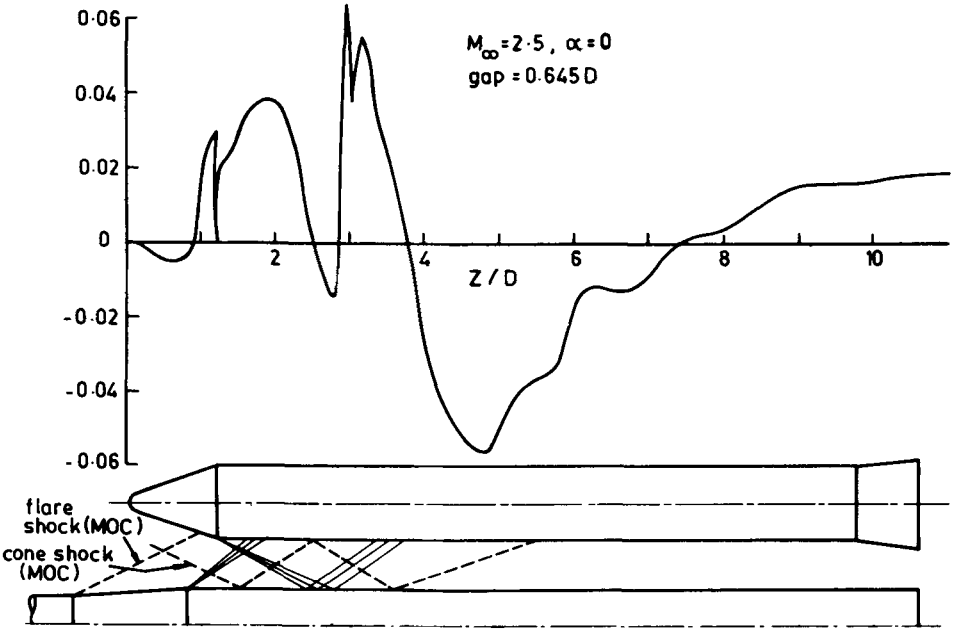

Figure 20. Aerodynamic load distribution on the strap-on; ordinate is (S/D_S) (dC_S/dz) where S is base area, D_S is the strap-on diameter and C_S is the side force coefficient.

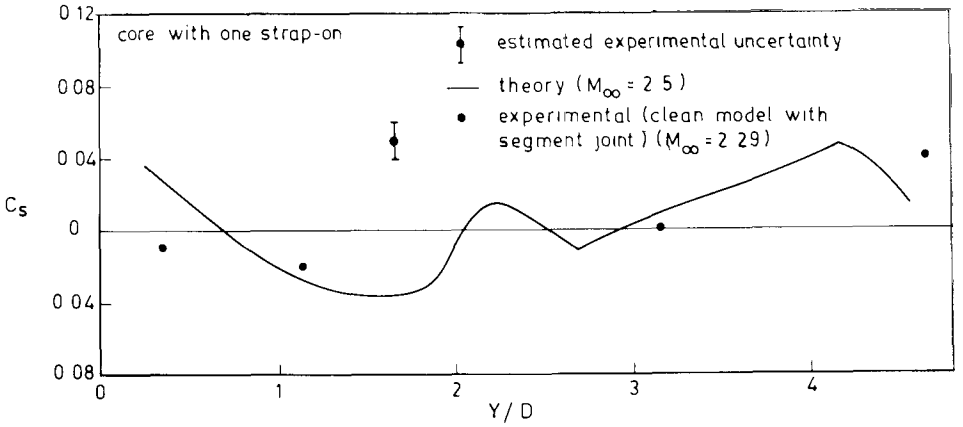

Figure 21. Variation of side force coefficient C_S of strap-on with lateral gap.

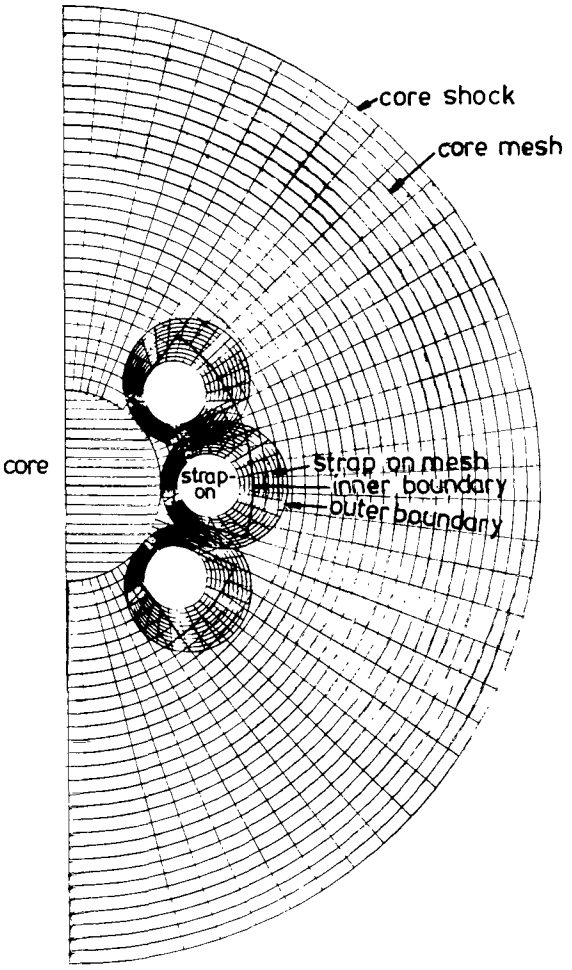

Figure 22. Overlap grid pattern for larger number of strap-ons as in PSLV.

layer. A typical shadowgraph picture of this interaction region is shown in figure 23, and boundary layer separation was indicated, as expected, for larger nose bluntness (Raja Kuperan 1982). The high overpressure observed in this region can also be seen in the figure.

3.3 *Transonic flows*

For tackling the transonic flow problem for a multi-body configuration like a strap-on launch vehicle, an attempt is being made to solve the full potential equations in cylindrical polar coordinates through a component adaptive grid approach (Jai Mohan 1986, unpublished). The grid adopted for the core and the strap-on with an overlap region is shown in figure 24. Some preliminary results

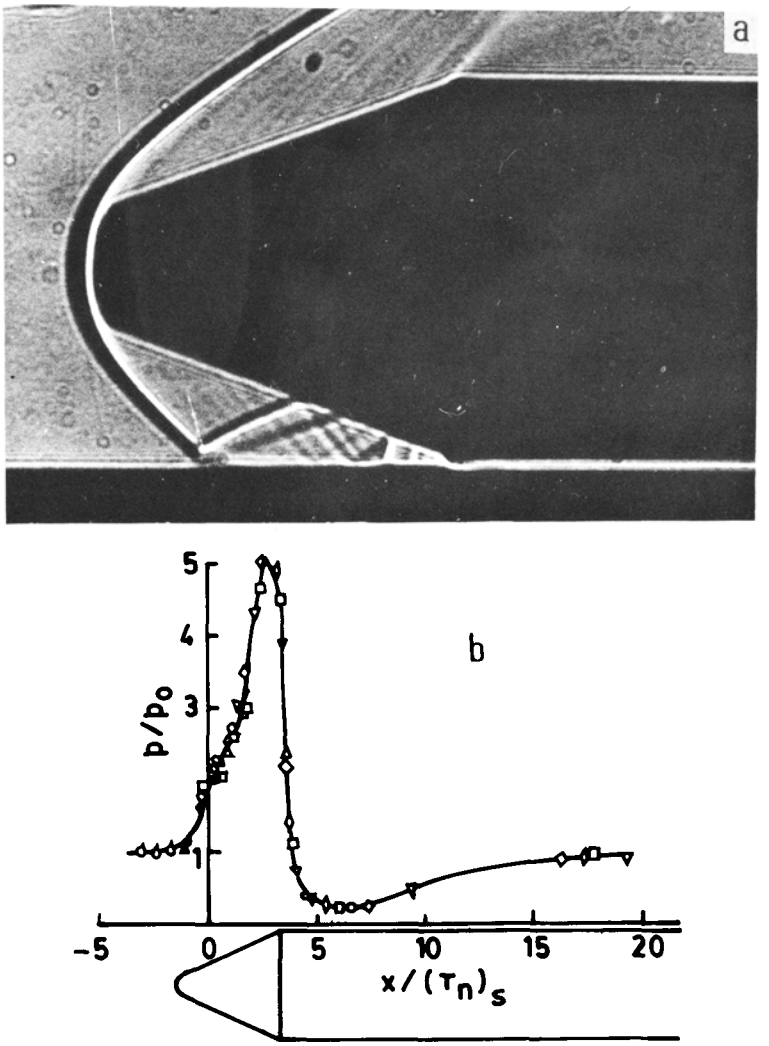

Figure 23. Strap-on shock interaction region; (**a**) Shadowgraph of shock reflections near strap-on booster nose. (**b**) Surface pressure distribution along the most windward generator of core-vehicle showing a region of high overpressure and the resultant high overpressure along the core body.

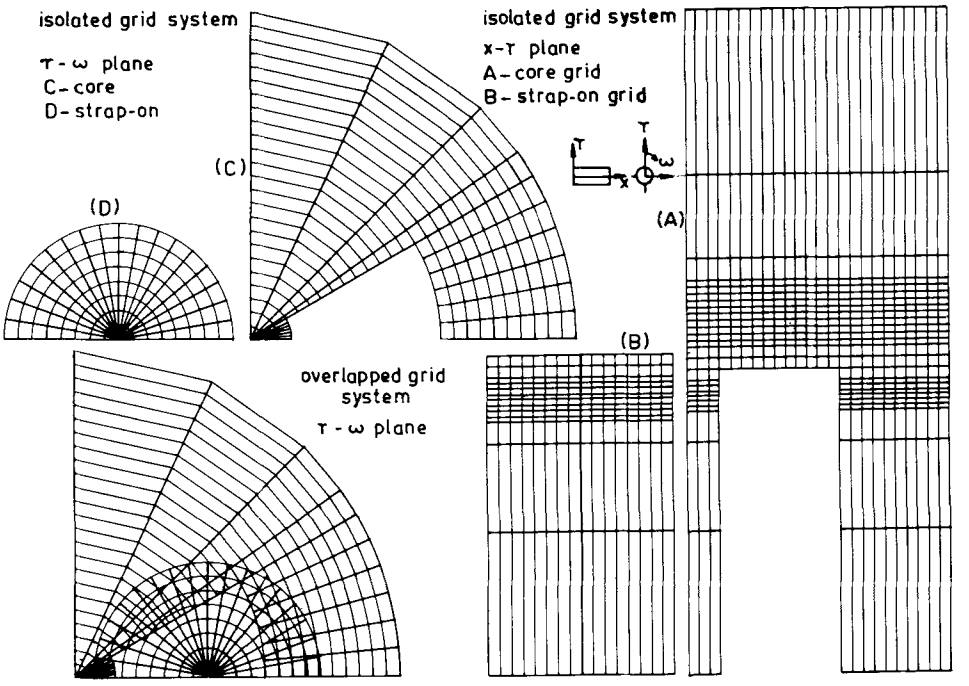

Figure 24. Component adaptive grid with overlap for core and strap-on for transonic full potential equation computation.

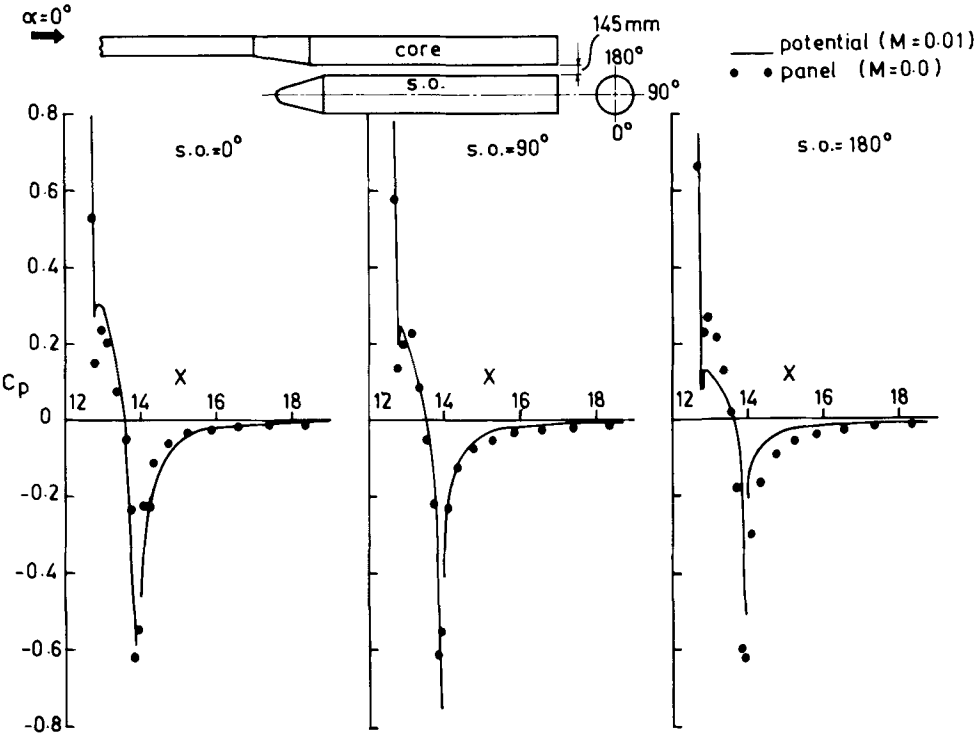

Figure 25. Preliminary results on pressure coefficient on strap-on using the full potential equation code in comparison with panel code results.

obtained for a low Mach number at zero incidence are compared with the incompressible panel method solution in figure 25 as a validation check for the code. Further work is in progress.

Efforts are also being made to extend the panel method to the solution of the full potential equation for transonic flow. This requires surface as well as field distribution of singularities and can involve large demands on computational time and memory for the three-dimensional case (K J Devassia 1986, private communication).

4. Strap-on separation

Laterally separating bodies pose a considerable challenge to analysis efforts when separation occurs during atmospheric flight, especially under supersonic Mach numbers and high dynamic pressure conditions (figure 26). Both ASLV and PSLV, one involving two strap-ons and the other involving six, have recently been considered.

While the initial separation force is imparted by an active system like a spring, the subsequent dynamics of the separating body is highly influenced by the complex aerodynamics involving both body interference and high incidence effects.

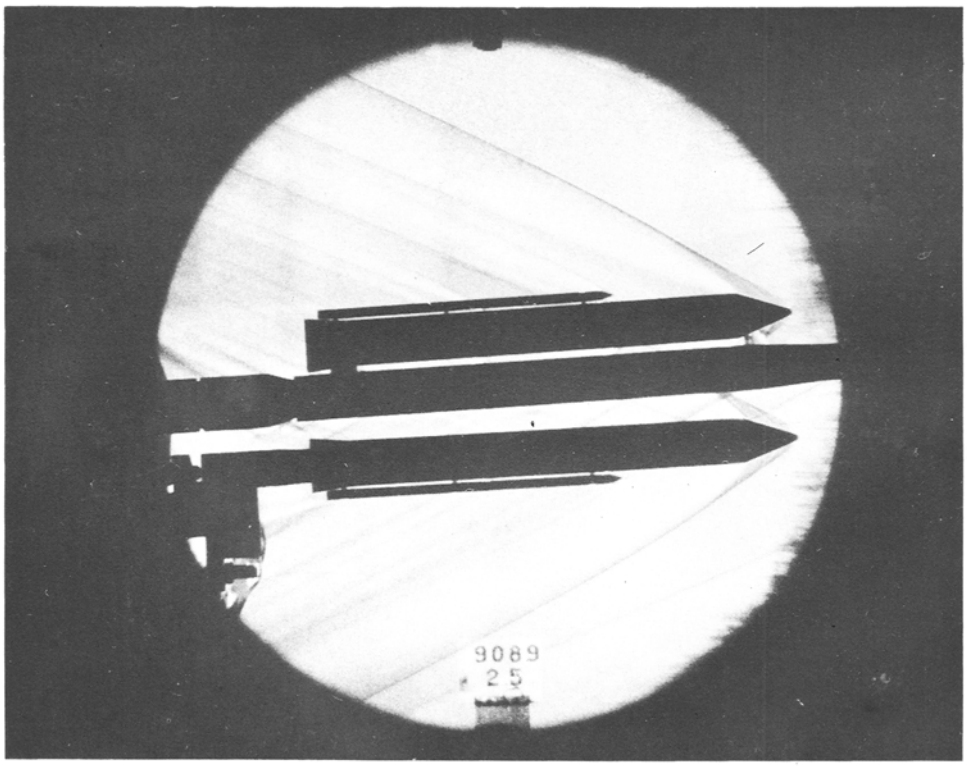

Figure 26. Schlieren picture indicating the flow field complexity during strap-on separation.

Analytical solution is extremely difficult and the wind-tunnel is pressed into service in a problem solving mode.

The investigation was conducted through a two-step approach in the 1·2 m trisonic wind-tunnel of the National Aeronautical Laboratory, Bangalore. At first, a coarse aerodynamic grid was generated using wind-tunnel measurements at fixed locations of the laterally separating body. The results were used for an approximate design of the separation system springs. This was followed by a more accurate time march analysis for the qualification of the design. Here the numerical simulation of the dynamics was done in an integrated fashion – though off line – using wind-tunnel results obtained at various steps of the separating trajectory for aerodynamic force and moment inputs (Sundara Murthy *et al* 1986).

Figure 27 shows the different positions of the separating strap-on booster of ASLV at various times when the vehicle is at zero incidence and figure 28 shows the effect of freestream incidence on the right and the left booster. Figure 29 represents one of the extreme cases where the worst combination of parameters like angle of incidence, tail off thrust etc. are considered. By an approximate analysis, it has been

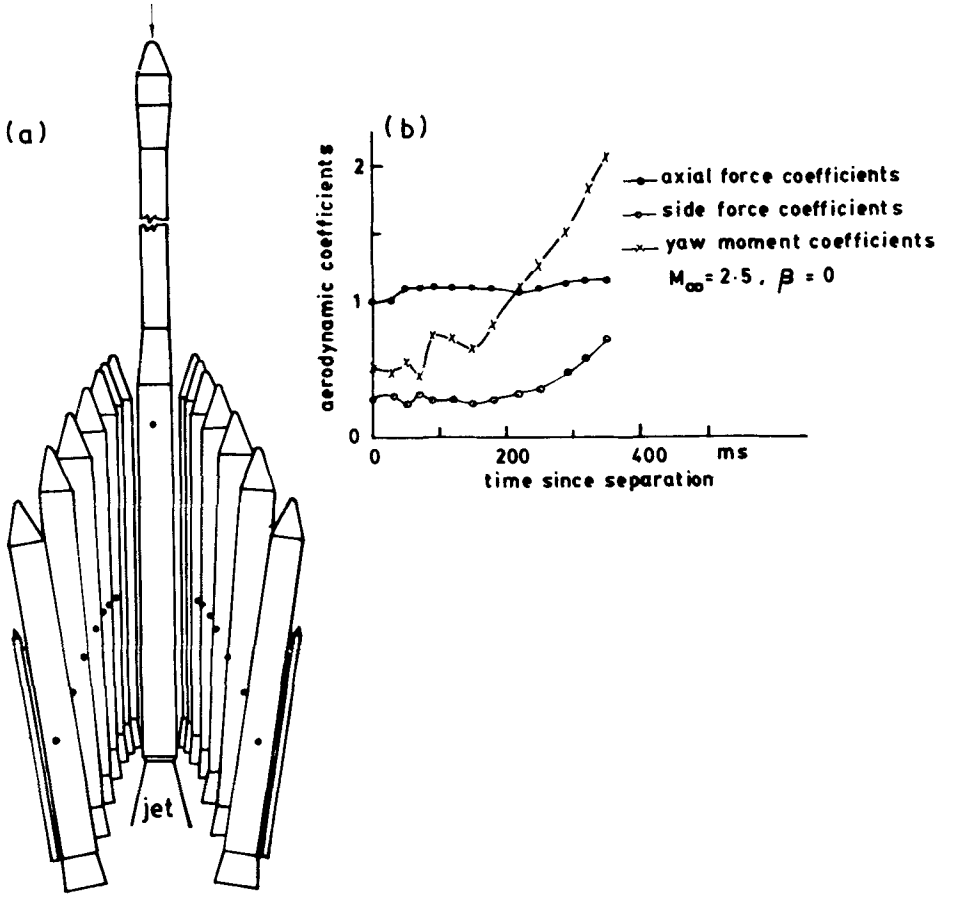

Figure 27. **(a)** Separation of strap-on booster at zero angle of incidence ($M_\infty = 2{\cdot}5$, $\beta = 0$) and **(b)** the corresponding aerodynamic coefficients.

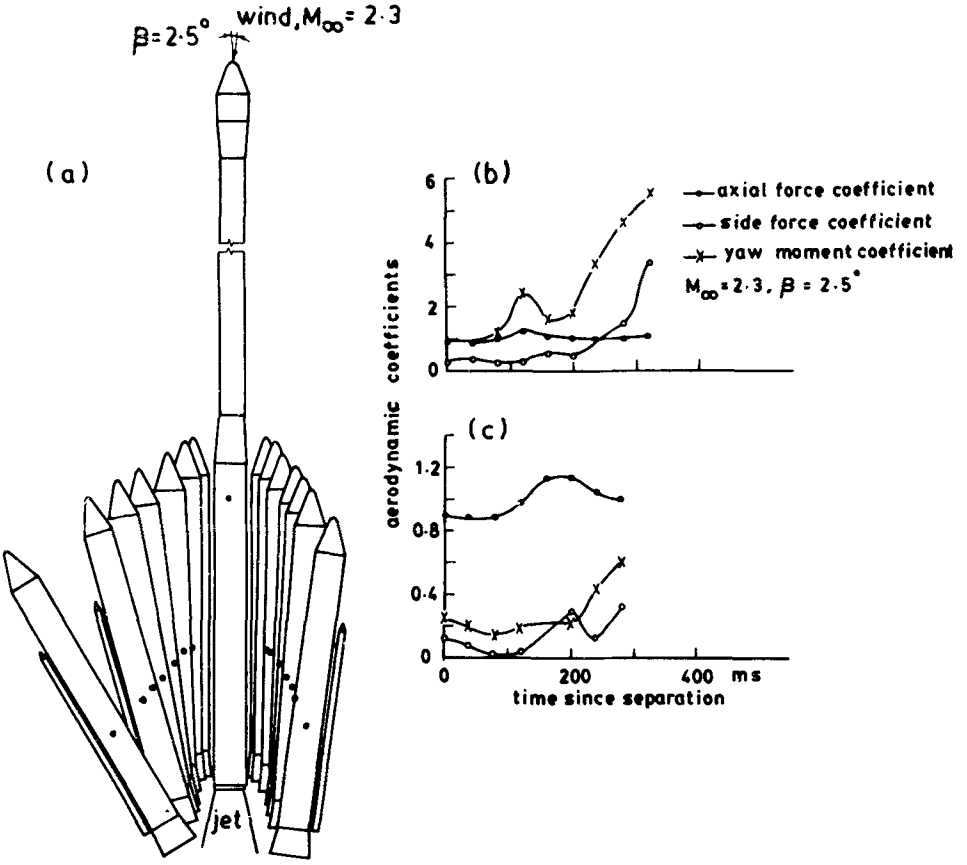

Figure 28. (a) Asymmetric separation of strap-on boosters at angle of incidence (yaw plane) ($M_\infty = 2{\cdot}3$, $\beta = 2{\cdot}5°$). The corresponding aerodynamic coefficients, (b) leeward booster, (c) windward booster.

verified that entry of the separating body into the core jet will not pose a serious problem.

The irregular variation of aerodynamic forces is also shown in these figures highlighting the complexity of the interference effects between the core and the separating strap-on. An attempt is being made to extend the Euler solution approach of §3·2 to the problem of the aerodynamnics of the separating strap-on.

5. Stage separation aerodynamics

The problem of stage separation flow interactions that arises during the atmospheric flight of multistage rockets is quite complex as can be seen in the schilieren picture shown in figure 30. Wind-tunnel tests for this purpose can be quite expensive, time consuming and difficult to conduct.

In order to capture all the physical features, an attempt is being made to simulate the flow field numerically using the full Navier-Stokes equations in the region of

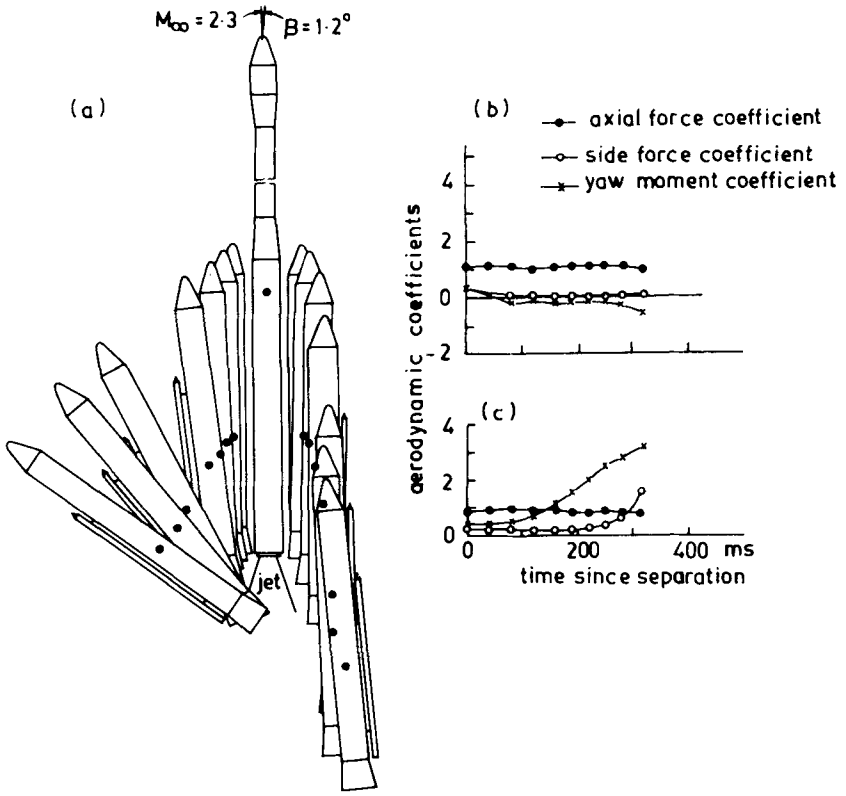

Figure 29. (a) Highly asymmetric separation of strap-on boosters under a severe off-nominal condition ($M_\infty = 2{\cdot}3$, $\beta = 1{\cdot}2°$). The corresponding aerodynamic coefficients for (b) windward booster, (c) leeward booster.

interest shown in figure 31. In the first phase, the time dependent problem has been tackled by employing the Fluid in Cell (FLIC) method (Saxena *et al* 1983). This has been applied to the simpler supersonic base flow problem as well as for the stage separation problem (laminar case), where the application of various boundary conditions, grids and convergence acceleration methods were tested out. Exponentially stretched grids and techniques of local time stepping and grid sequencing were found to result in a considerable saving in computational time. Figure 32 shows the FLIC solution for the base flow problem with supersonic jet and freestream.

However, this study brought out that even though qualitatively good results could be obtained through conventional FLIC, it could result – being first-order accurate – in large numerical damping which competes with the physical viscosity in separated flow and viscous-inviscid interaction regions leading to highly smeared shocks.

To eliminate these limitations, the second-order accurate MacCormack's explicit scheme with operator splitting was tried in the second phase of the work. However, a final decision was taken to go for the state-of-art implicit techniques because of the very large CPU times that would be required on the VSSC CDC 170/730 computer system for the high Reynolds number Navier-Stokes solutions by the explicit

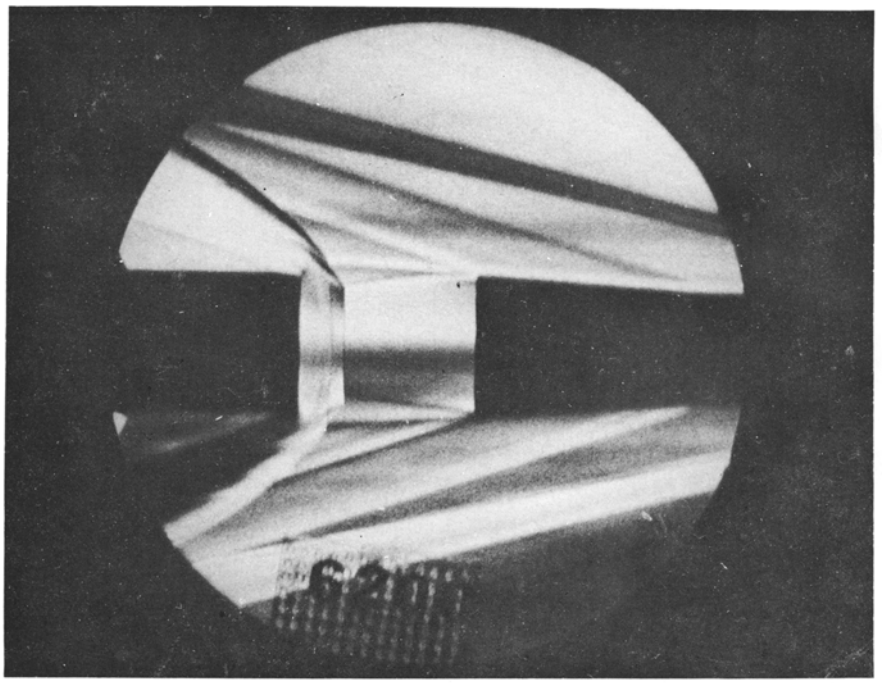

Figure 30. Schilieren picture of stage separation with separating booster (left) in the vicinity of sustainer (right) jet.

method. Work also has been done in improving the conventional FLIC method and making it second-order accurate and thus competitive with the other methods mentioned above (Saxena 1986).

6. Boat tail aerodynamics

In many launch vehicles, the payload shroud has to be larger in diameter compared to the rest of the vehicle in order to accommodate payloads of larger volumes. This leads to bulbous (or hammerhead) configurations which are susceptible to problems like transonic buffet, shock wave-boundary layer interactions, local flow separations etc. Some of these problems of both steady and unsteady nature are under investigation at VSSC.

6.1 *Supersonic flow*

Aerodynamic loading distributions computed through a simple second-order shock expansion approach (Goyal 1981) are shown in figure 33 for PSLV and ASLV forebodies along with experimental results. An equivalent body concept is used wherein each meridian is defined by an equivalent axisymmetric body at zero incidence. A three-dimensional inviscid flow field solution on such bodies at the angle of incidence is also obtained by the shock capturing finite difference Euler

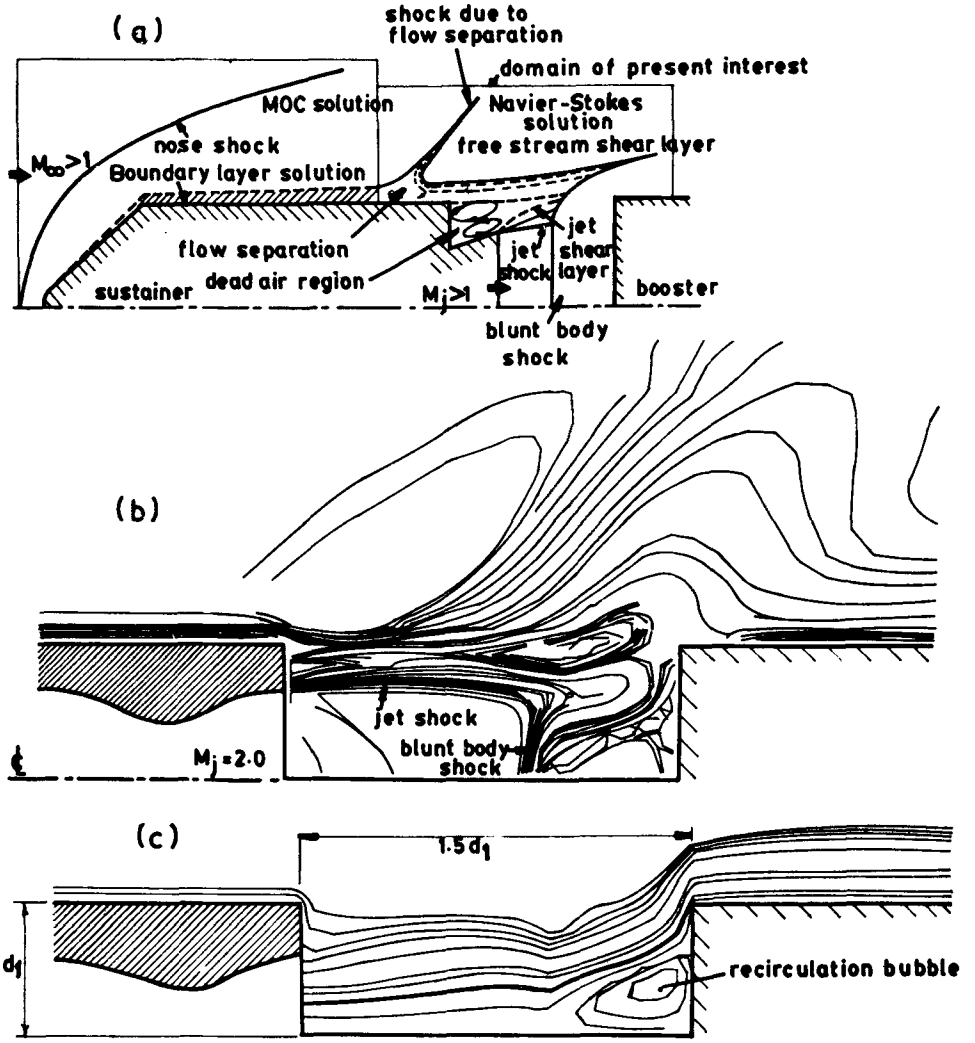

Figure 31. Numerical simulation of jet on-stage separation aerodynamics through FLIC (fluid in cell method); Free stream Mach number = 2·0, jet Mach number = 2·0, exit jet to base diameter = 0·6, Reynolds number based on length upto base = $0{\cdot}4 \times 10^6$, specific heat ratio = 1·4, (a) General configuration and domain of present interest, (b) Constant Mach number contours, (c) Streamline plot.

solver (Singh & Rajaram 1985) with grid clustering close to the body to resolve the entropy layer. A typical result is shown in figure 34.

A supersonic flow field simulation has also been attempted for the boat-tailed payload shroud of PSLV through a time-dependant Reynolds averaged Navier-Stokes code (Purohit 1986b) using the Baldwin & Lomax (1978) turbulence model. Figure 35 shows a 1/80th scaled down model (used for wind-tunnel tests) and the grid system employed with clustering of grids near the surface and around the boat tail. Pressure distributions obtained at various Mach numbers 1·80, 2·47, 3·0 and 3·5 from the computational code are compared with experimental results at zero

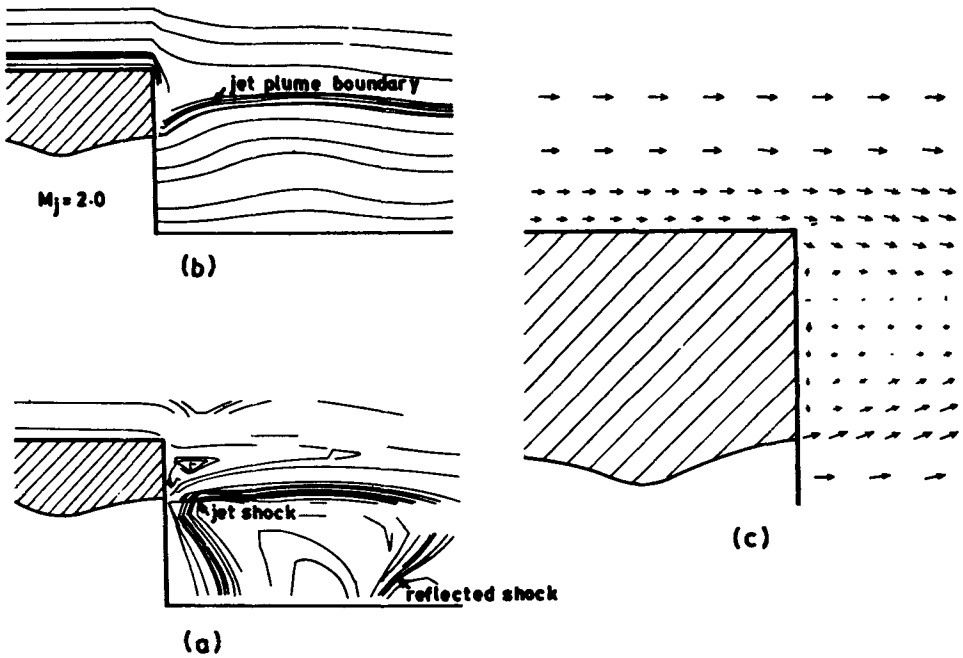

Figure 32. Numerical simulation of base flow with jet through FLIC (Fluid in cell method); Conditions same as in figure 31. (a) Constant Mach number contours. (b) Streamline plot. (c) Velocity plot.

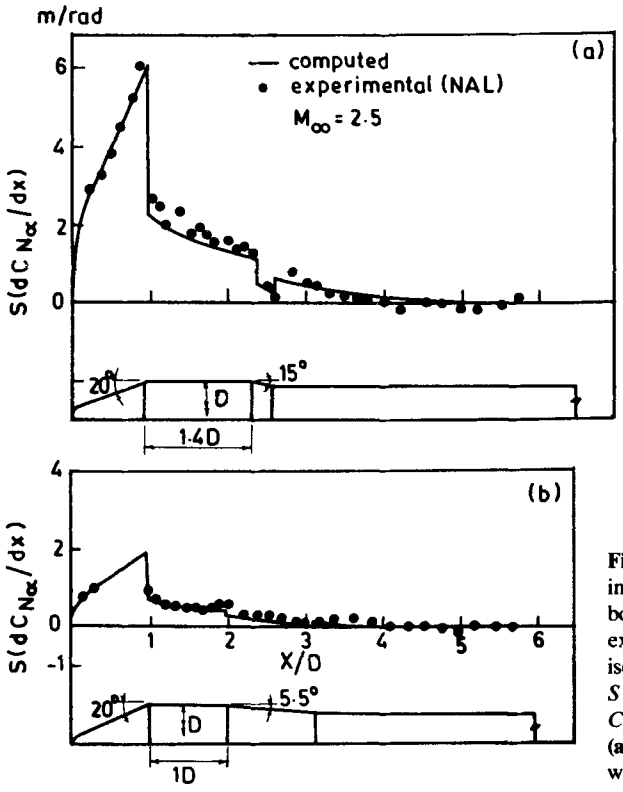

Figure 33. Aerodynamic loading distributions on boat-tailed bodies through second-order shock expansion approach in comparison with experimental results; S = reference area based on D, C_N = normal force derivative. (a) PSLV with $D = 3{\cdot}2$ m. (b) ASLV with $D = 1$ m.

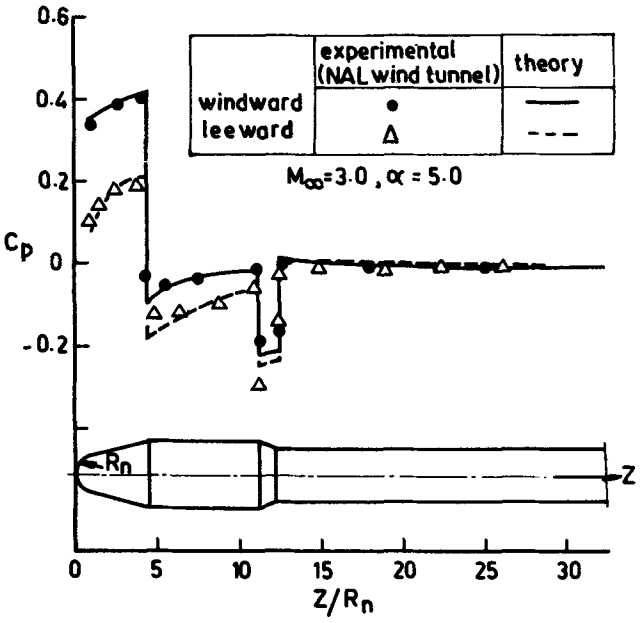

Figure 34. Pressure coefficient on a boat-tailed body in supersonic flow at incidence obtained from shock capturing finite difference Euler solver in comparison with experimental results.

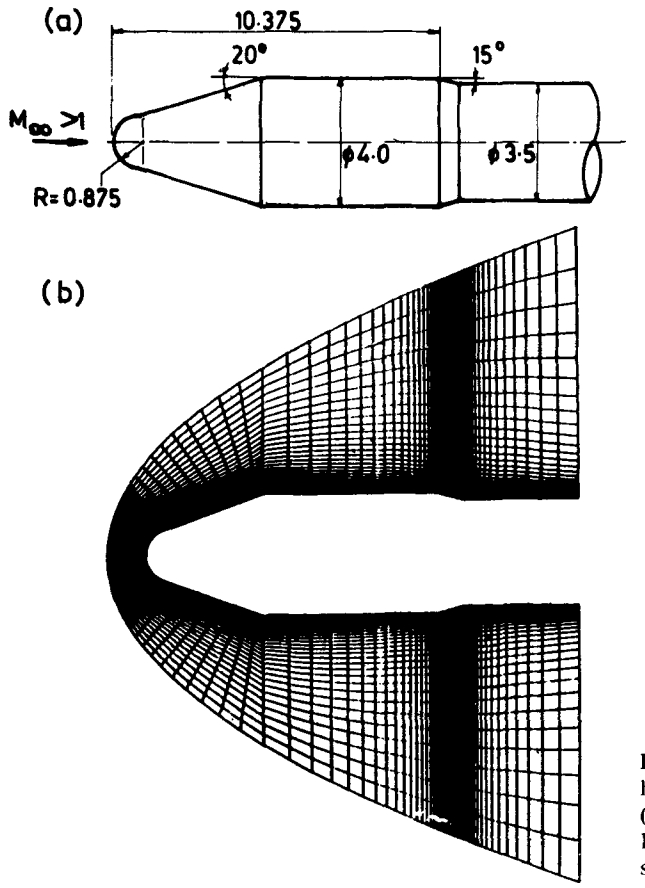

Figure 35. (a) The boat-tailed heat shield configuration and (b) the grid system used for the Reynolds-averaged Navier-Stokes solution.

incidence in figure 36. Details of the velocity field near the boat tail and shock strengths for various Mach numbers are shown in figure 37. From this, it is seen that the flow is separated upto Mach number 2·47 beyond which it is attached. The observation is further substantiated by the skin friction plots along the boat tail shown in figure 38. At $M = 2{\cdot}47$, the condition of incipient separation prevails.

6.2 *Transonic flow*

Transonic flow calculations have been performed for a boat-tailed body using the full potential equations (Jai Mohan 1985). In the boat-tailed region, where viscous effects are important, an axisymmetric viscous bump model is introduced at the shock foot in the inviscid calculation. This solves the integral boundary layer equations, using as initial conditions the local flow upstream of the shock, and the total flow field is simulated in an interactive manner. A typical comparison with experimental results is shown in figure 39.

An attempt has been made to tackle the transonic unsteady flow problem over a boat-tailed configuration using theunsteady Reynolds averaged Navier-Stokes code mentioned earlier (Purohit 1986a). Figure 40 shows the body considered and the grid system used. It also shows a comparison of the steady state results obtained from the computation with the experimentally obtained pressure coefficient C_p for

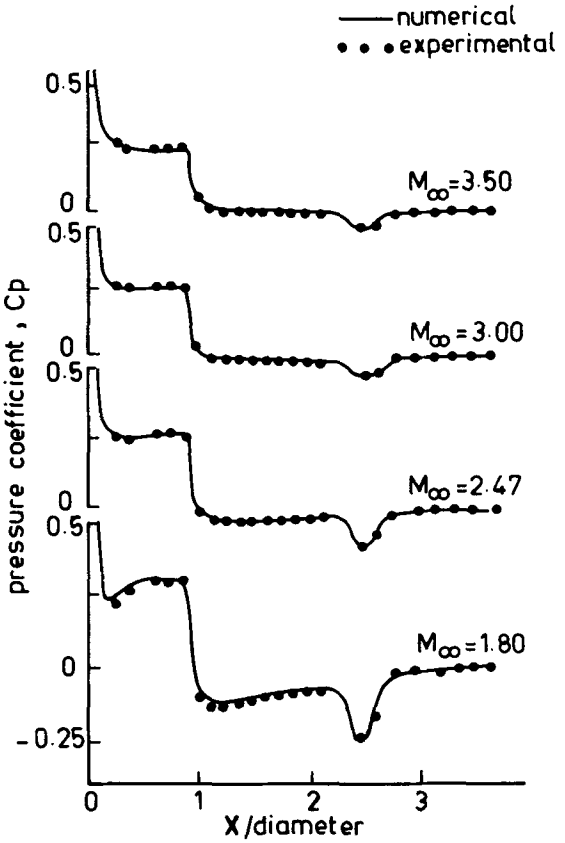

Figure 36. Pressure coefficient along the length of the body obtained through Navier-Stokes solver in comparison with experimental results.

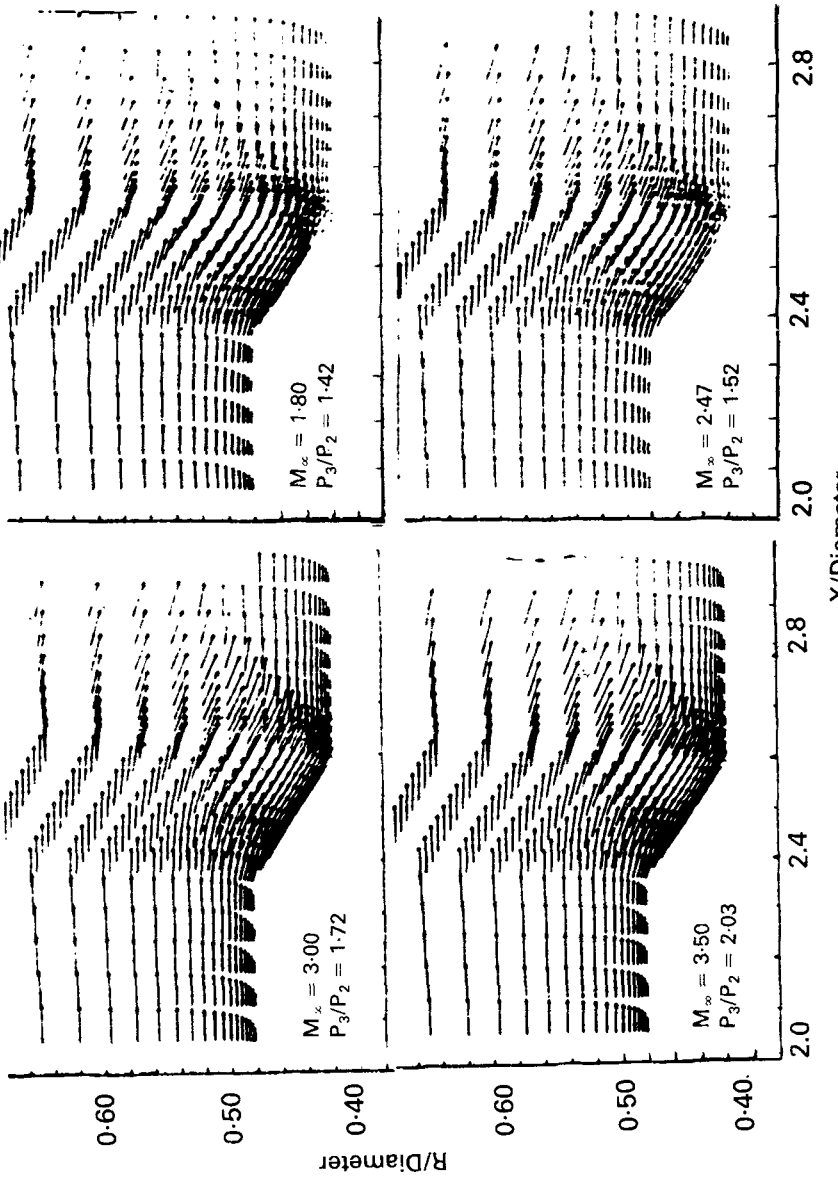

Figure 37(a). Flow field along boat-tail junction for various Mach numbers.

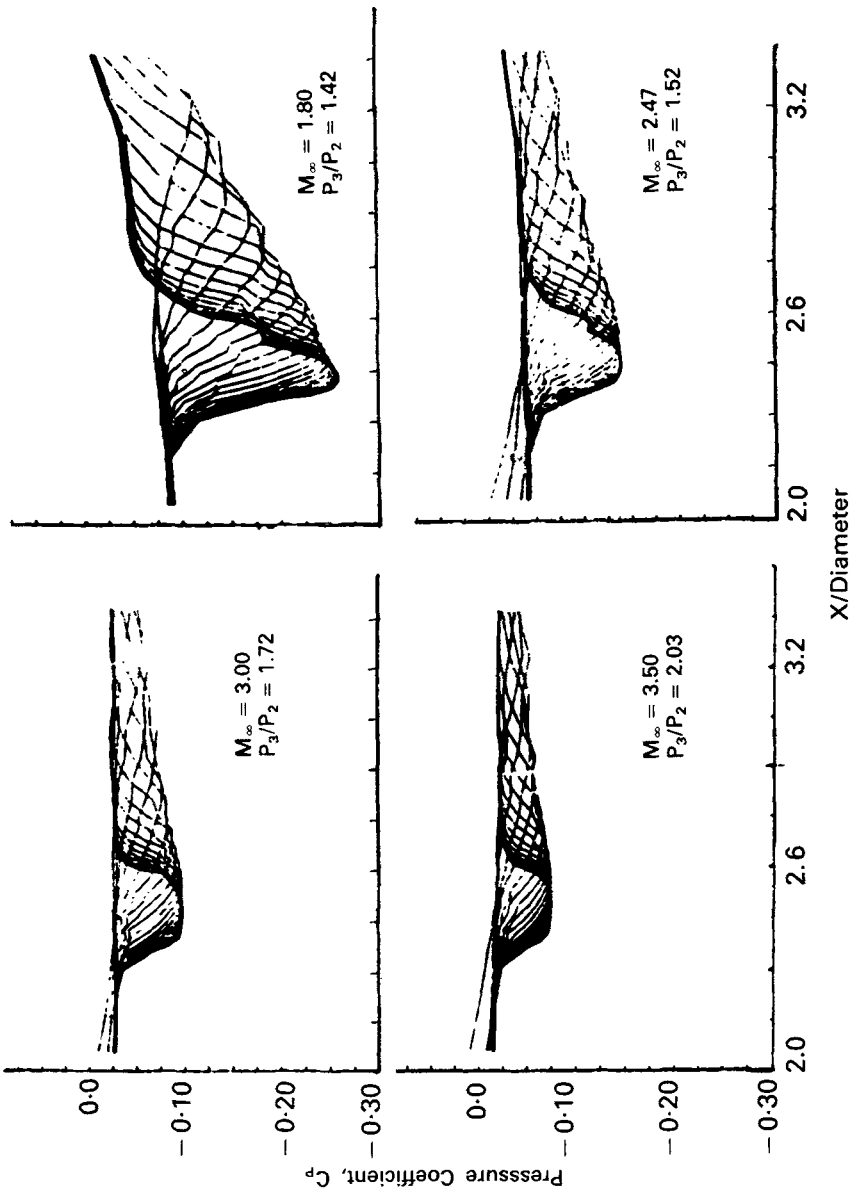

Figure 37(b). Shock strengths for Mach numbers corresponding to those of figure 37a.

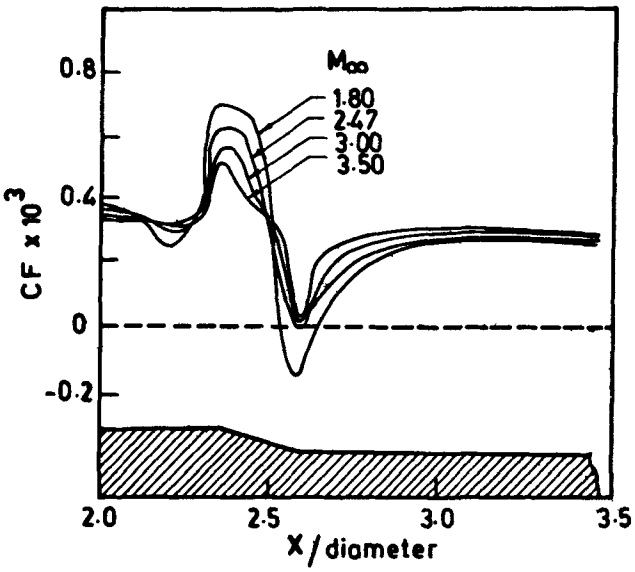

Figure 38. Skin friction coefficient along boat tail showing incipient separation condition at $M = 2{\cdot}47$.

a Mach number of 0·8 and a Reynolds number of 10^6/metre. From the unsteady surface pressure data shown in figure 41, sound pressure levels (SPL) are evaluated at various locations on the payload shroud. As can be seen in the figure, a maximum SPL of 152 dB at a frequency of 300 Hz was resolved at $X/D = 1{\cdot}08$. Highest credible frequency of the numerical analysis was 14·8 kHz which can be

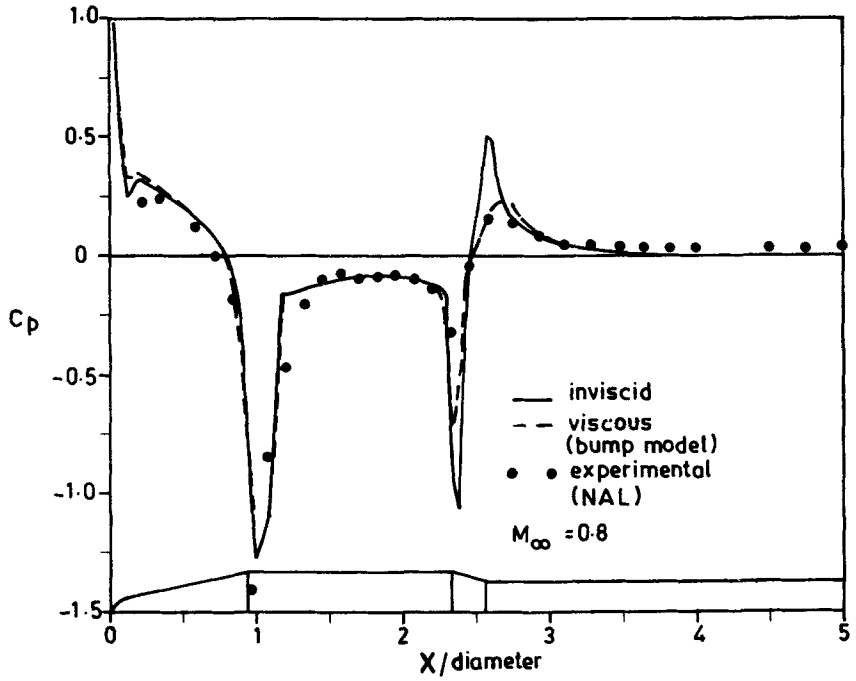

Figure 39. Transonic pressure distribution on a boat-tailed configuration with viscous correction through 'bump model'.

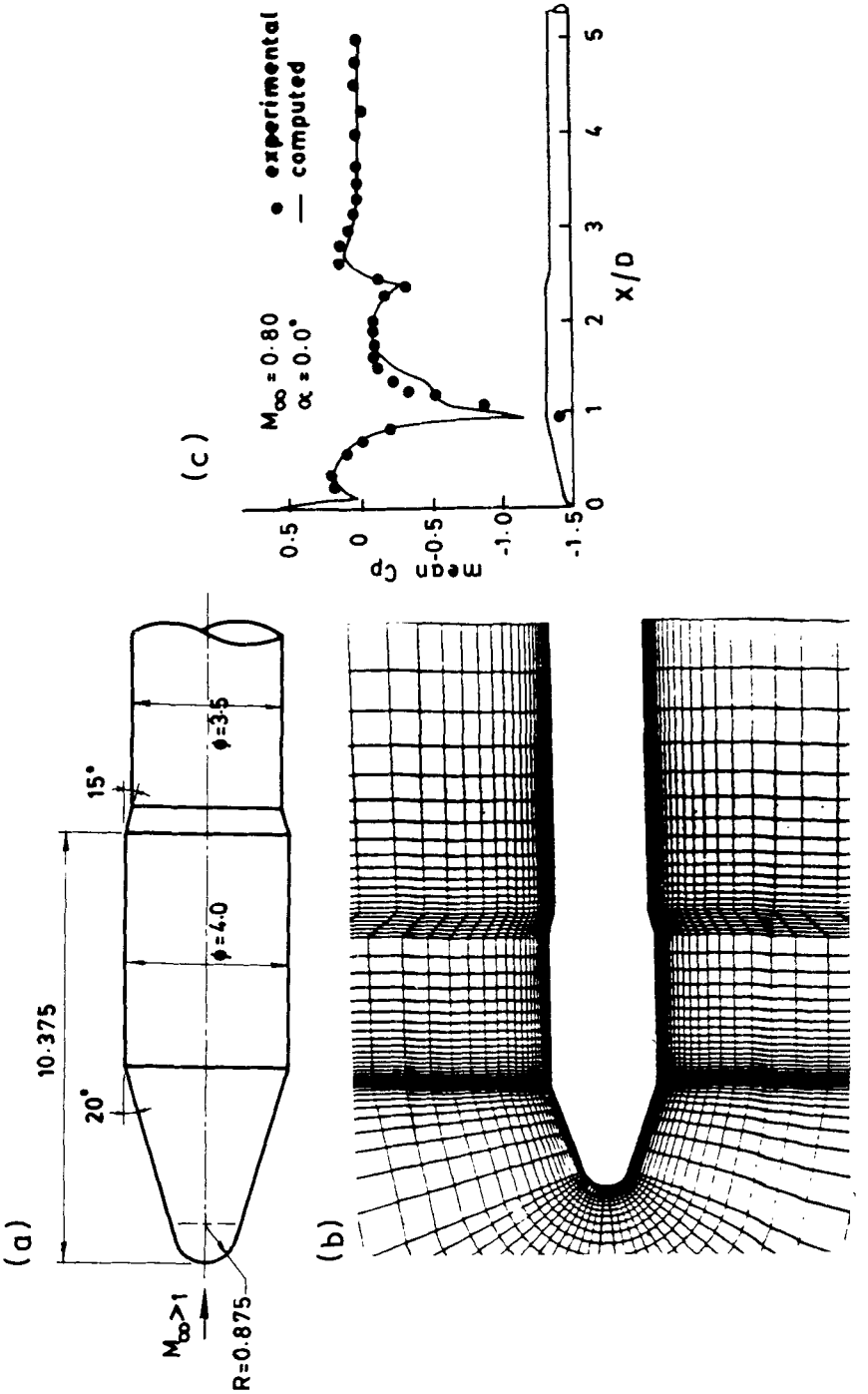

Figure 40. (a) Body and (b) grid system for a boat for transonic flow computation through unsteady Reynolds-averaged Navier-Stokes code; (c) comparison of steady state pressure distribution with experimental results.

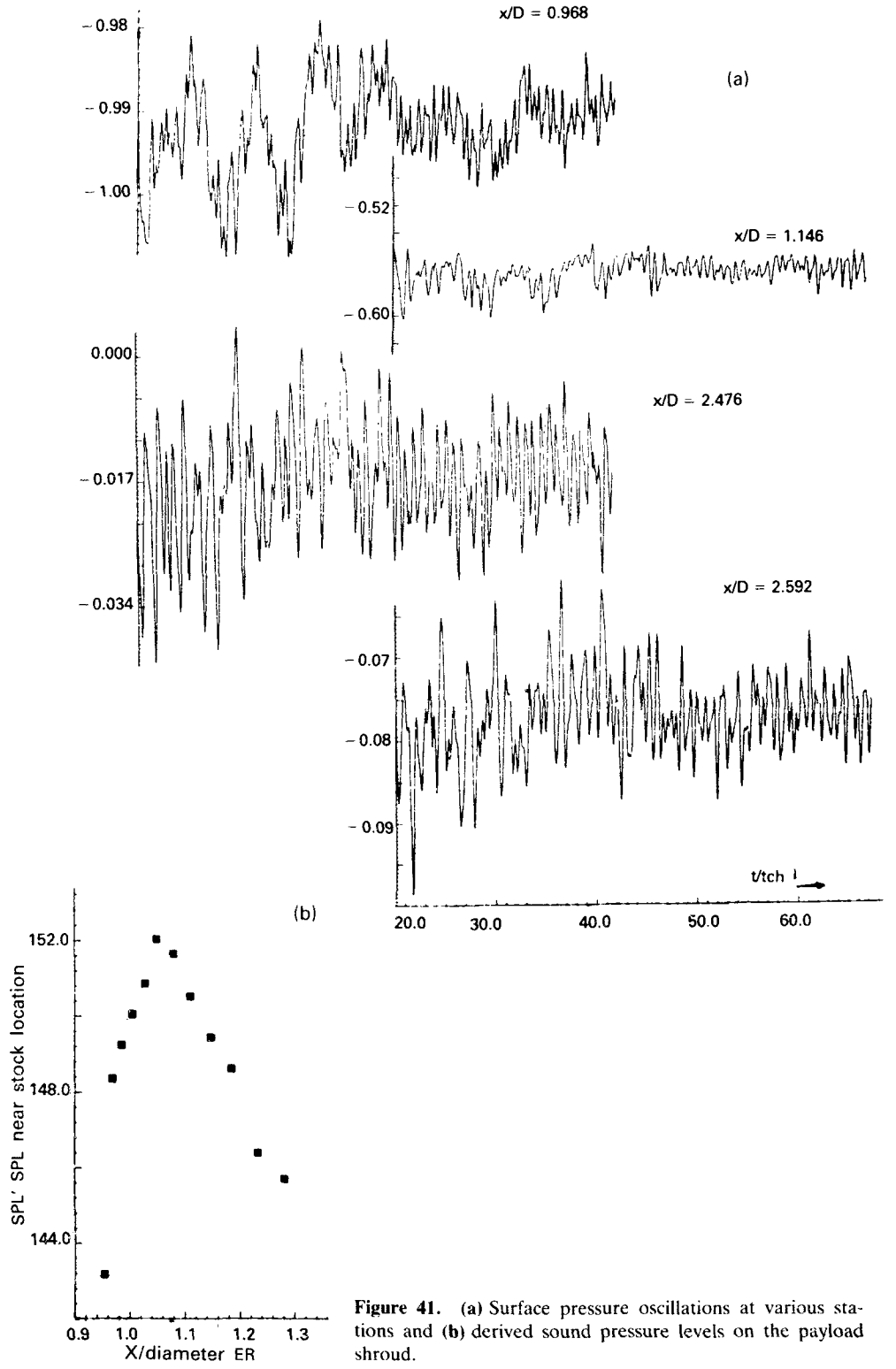

Figure 41. (**a**) Surface pressure oscillations at various stations and (**b**) derived sound pressure levels on the payload shroud.

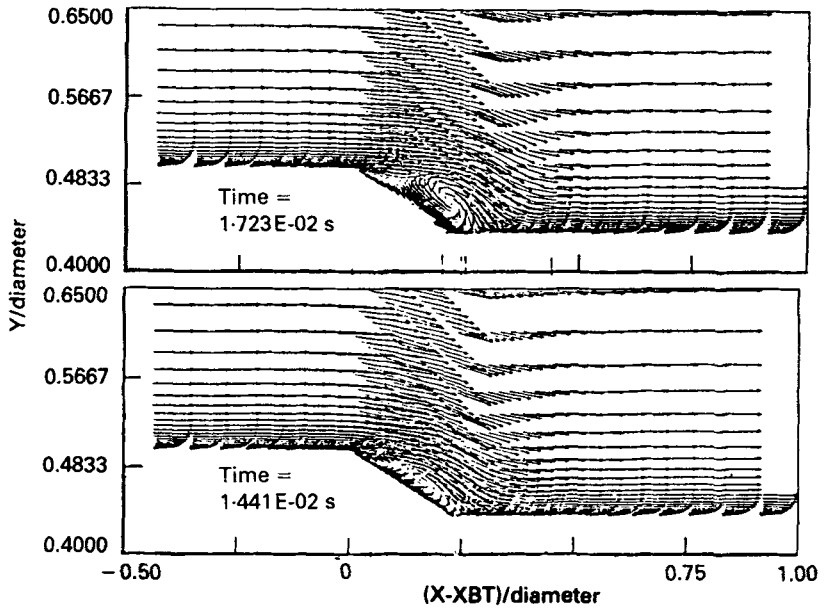
0.6500
0.5667
0.4833
0.4000
Time =
1·723E-02 s
0.6500
0.5667
0.4833
0.4000
Time =
1·441E-02 s
Y/diameter
−0.50
0
0.75
1.00
(X-XBT)/diameter

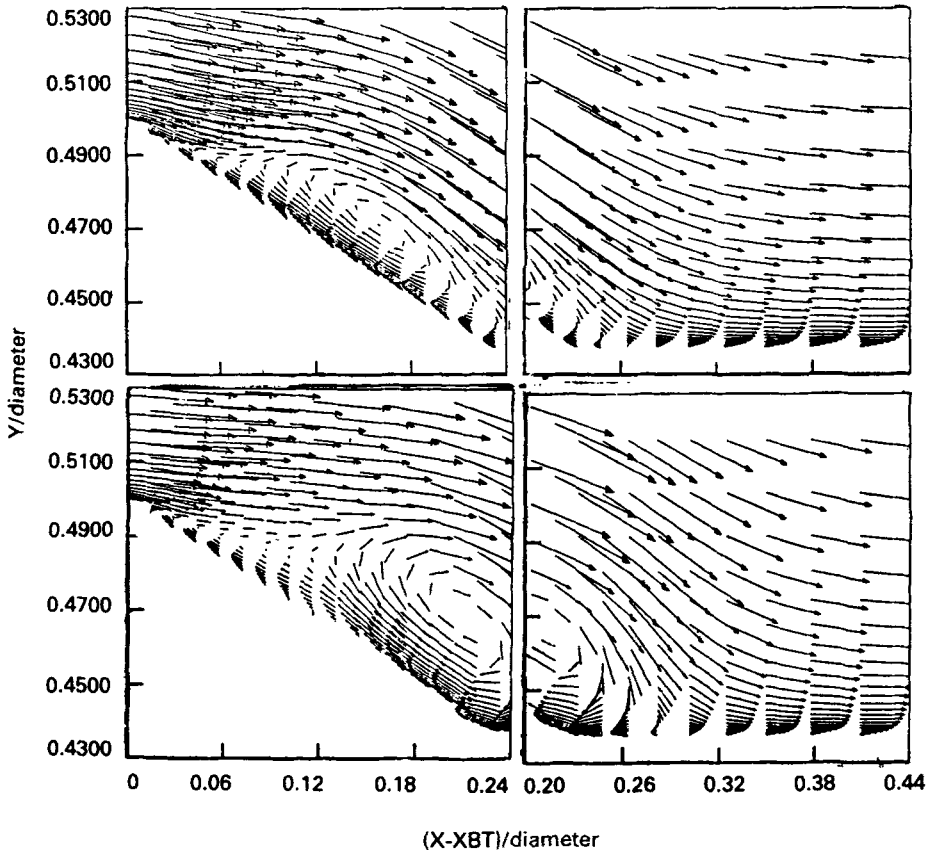
0.5300
0.5100
0.4900
0.4700
0.4500
0.4300
0.5300
0.5100
0.4900
0.4700
0.4500
0.4300
Y/diameter
0
0.06
0.12
0.18
0.24
0.20
0.26
0.32
0.38
0.44
(X-XBT)/diameter

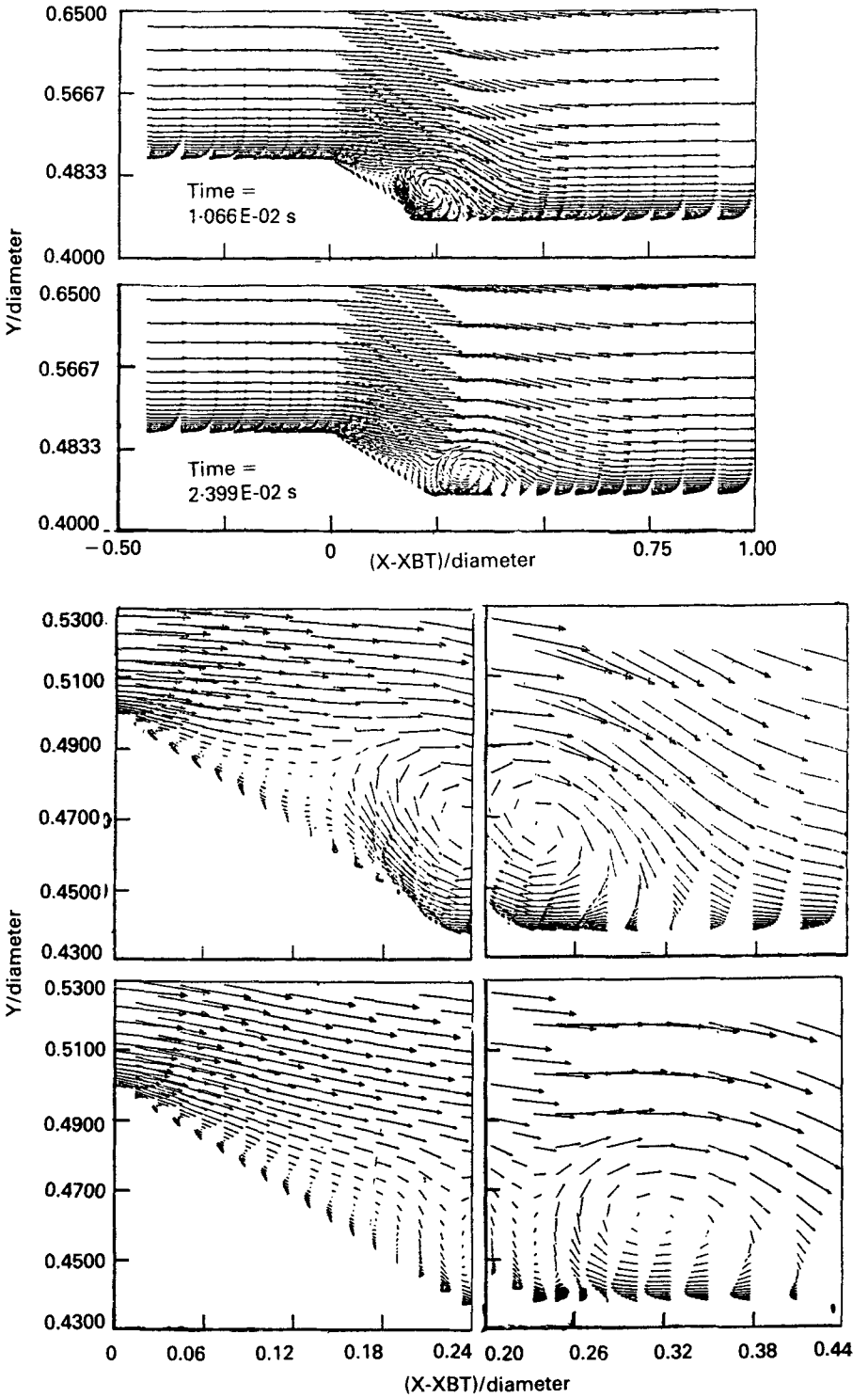

Figure 42. Capture of vortical motion in the boat-tailed region through Navier-Stokes code. The right hand portion is the flowfield in the boat-tailed region in enlarged scale.

improved by considering a finer mesh. Also, the initiation and development of vertical motion caused by boundary layer separation at the boat-tail corner is captured by the time-dependent calculation as shown in figure 42.

Unfortunately, these unsteady flow computations had to be restricted to the zero incidence case because of computer limitations in considering the additional circumferential variation that occurs at the angle of incidence, even though the code is capable of handling the 3*D* problem. Further, an approach of this type which uses Reynolds averaged equations with a steady state turbulence model is expected to capture relatively low frequency phenomena like shock oscillations during transonic buffet. Through this approach, it may not be possible, however, to capture accurately the high frequency content of aerodynamic noise.

7. Concluding remarks

Some of the important aerodynamic problems associated with satellite launch vehicles under development in India, which have features like strap-on boosters, bulbous payload shrouds etc., are identified and the work being done at VSSC for tackling these problems is discussed. Generally these problems are quite complex and are of three-dimensional nature. While the rapidly emerging field of computational fluid dynamics (CFD) can play a very significant role, it is essential that an integrated approach involving analytical, computational and experimental methods is used for obtaining practical design solutions and a comprehensive understanding of many of these complex problems.

References

Anon 1985 Configuration design of jet deflector for PSLV launch pad system, VSSC:ADDG:TR:1:85, Aerospace Dynamics and Design Group, Vikram Sarabhai Space Centre, Trivandrum, January

Baldwin B S, Lomax H 1978 Thin layer approximation and algebraic model for separated turbulent flows, AIAA Paper, 78–257, January 1978

Devassia K J, Nair S R, Sheo Prakash 1982 *Proceedings of the Thirteenth International Symposium on Space Technology and Science* (Tokyo: AGNE Publishers)

Goyal V K 1981 Cylinder effects on aerodynamic loading of following boat tail and cylinder combination at supersonic speed, VSSC:TN:02:045:81, Aerodynamics Division, VSSC, Trivandrum, October

Jai Mohan 1985 Simulation of shock-boundary layer interaction effects in transonic potential flow, VSSC-ADDG-ARD-002, Aerodynamics Division, VSSC, Trivandrum, July

MacCormack R W 1969 The effect of viscosity in hypervelocity impact cratering, AIAA Paper No. 69–354

Prasad J K, Kutty C S 1985 Impingement on PSLV jet deflector: cold flow simulation test results, VSSC:ATTF:07:85, Aerothermal Test Facilities, VSSC, Trivandrum, October

Purohit S 1986a Numerical simulation of transonic flow past bulbous heat shield, Proceedings of the Third Asian Congress of Fluid Mechanics, September 1–5, 1986, Tokyo, Japan

Purohit S 1986b Supersonic flow simulation for a boat tailed heat shield, Accepted for publication in The Aeronautical Journal, Royal Aeronautical Society, London

Raj Kuperan E 1982 Experimental investigation for strap-on launch vehicle at supersonic regime, VSSC:SSTC:ARD, Aerodynamics Division, VSSC, Trivandrum, November

Saxena S K 1986 *Development and typical assessment of a new flick method for base flows*, PhD thesis (submitted), Indian Institute of Science, Bangalore

Saxena S K, Deshpande S M, Narasimha R, Prahlad T S 1983 Numerical Simulation of base flow, Proceedings of the Second Asian Congress of Fluid Mechanics, Beijing, China, 25–29 October, 643–648

Singh K P, Deshpande S M, Prahlad T S, Narasimha R 1987 Numerical simulation of inviscid supersonic flow over a launch vehicle with strap-on boosters, AIAA 25th Aerospace Sciences Meeting, Reno, Nevada, January 12–15

Singh K P, Rajaram U 1985 Numerical simulation of three-dimensional inviscid supersonic flow over launch vehicles, VSSC-ADDG-009, Aerodynamics Division, VSSC, Trivandrum, December

Sundara Murthy H, Narayana K Y, Suryanarayana G K, Rajeev Lochan, Sasidharan Nair K G, Varabally B S 1986 *J. Aeronaut. Soc. India* (Special Issue on Second National Conference on Aerodynamics, December 1986, Bangalore) (submitted). 38: 215–221